

PHYSICAL REVIEW D

PARTICLES AND FIELDS

THIRD SERIES, VOLUME 35, NUMBER 12

15 JUNE 1987

Superconducting gravity gradiometer for sensitive gravity measurements. I. Theory

H. A. Chan* and H. J. Paik

Department of Physics and Astronomy, University of Maryland, College Park, Maryland 20742

(Received 1 July 1986)

Because of the equivalence principle, a global measurement is necessary to distinguish gravity from acceleration of the reference frame. A gravity gradiometer is therefore an essential instrument needed for precision tests of gravity laws and for applications in gravity survey and inertial navigation. Superconductivity and SQUID (superconducting quantum interference device) technology can be used to obtain a gravity gradiometer with very high sensitivity and stability. A superconducting gravity gradiometer has been developed for a null test of the gravitational inverse-square law and space-borne geodesy. Here we present a complete theoretical model of this instrument. Starting from dynamical equations for the device, we derive transfer functions, a common mode rejection characteristic, and an error model of the superconducting instrument. Since a gradiometer must detect a very weak differential gravity signal in the midst of large platform accelerations and other environmental disturbances, the scale factor and common mode rejection stability of the instrument are extremely important in addition to its immunity to temperature and electromagnetic fluctuations. We show how flux quantization, the Meissner effect, and properties of liquid helium can be utilized to meet these challenges.

I. INTRODUCTION

Highly sensitive gravity sensors are needed to investigate fundamental properties of gravitation and to improve accuracies of gravity survey and inertial navigation. Torsion balances have been used over two centuries for sensitive gravity experiments.¹ Spring-mass, pendulum, and free-fall-type gravimeters² have been developed as survey instruments as well as a superconducting version of the first type.³ Research to develop detectors for gravitational waves of extraterrestrial origin has started over two decades ago.⁴ Cryogenic mass-quadrupole-type and laser-interferometer-type detectors are under vigorous development.⁵ The last two decades have also seen dedicated efforts to develop room-temperature gravity gradiometers⁶⁻⁸ for moving-base survey applications. Superconducting gravity gradiometers have emerged more recently as an outgrowth of the superconducting transducer work for low-temperature gravitational-wave detectors.⁹

The extremely weak nature of gravitational interaction poses a challenge to the state of the art technology for signal transduction and amplification as well as isolation of environmental noise. To compound the problem, the gravitational field cannot be distinguished in a *local* measurement from acceleration of the reference frame by the equivalence principle. In order to separate gravity from frame accelerations, one must resort to a *second-order*

measurement using the tensor nature of gravitational field gradient or "gravity gradient." When the platform is undergoing a linear acceleration, a differential measurement over a base line between two proof masses will cancel out the acceleration noise, leaving gravity to be detected as the signal. Likewise, an angular acceleration can be taken out by combining signals from four proof masses as we will see in Sec. II. Thus, unlike in electromagnetism, where a single test charge can be used to determine the field uniquely, a tidal-force sensor or a "gradiometer" is the *fundamental* instrument in gravity which is capable of measuring its field, independent of platform motion. True acceleration measurement, in turn, requires removal of gravity noise which again calls for the use of a gravity gradiometer. It is therefore not surprising to find that instruments employed in most precision gravity experiments, such as torsion balances and Weber-type gravitational-wave detectors, have actually been special types of gradiometers.

The acceleration difference along the direction j per unit separation along the direction i is defined to be the ij component of the gravity gradient tensor $\vec{\Gamma}$:

$$\Gamma_{ij}(\mathbf{r}, t) \equiv -\frac{\partial^2 \phi(\mathbf{r}, t)}{\partial x_i \partial x_j}, \quad (1)$$

where $\phi(\mathbf{r}, t)$ is the gravitational potential. A very weak

gradient of 1 nm sec^{-2} per m is equal to one Eötvös (E) unit, defined by

$$1 \text{ E} \equiv 10^{-9} \text{ sec}^{-2}. \quad (2)$$

Many ground-based survey applications call for such high sensitivity. Geodesy application in space requires even higher sensitivity at the level of $10^{-4} \text{ E Hz}^{-1/2}$ (Ref. 10). The extreme weakness of gravitational interaction and the practical difficulties associated with balancing out the acceleration noise to a sufficient degree have *limited* the sensitivity of room-temperature gradiometers to a level of $1-10 \text{ E Hz}^{-1/2}$ (Ref. 10). Major improvements in sensitivity and stability are expected of the superconducting devices under development. It appears that a superconducting gravity gradiometer of a relatively compact design will have a sufficient sensitivity for space applications.

Besides possessing low thermal noise and low mechanical drift as direct consequences of a cryogenic temperature, the new gradiometer takes advantage of many exotic properties of superconductivity. Quantized magnetic flux is used as an extremely stable tool to achieve transducer action and common mode balance. Operating at liquid-helium temperatures, a SQUID (superconducting quantum interference device) serves as the most sensitive amplifier of today. Superconductivity can be used to make a nearly perfect electromagnetic shield and superfluid helium can provide a stable, gradient-free temperature environment. Flux quantization can further be used to accomplish stable levitation of proof masses against gravity in a terrestrial environment and to enhance the gradiometer sensitivity by means of a "superconducting negative spring."¹¹

Two schemes (*current differencing* and *displacement differencing*) of a superconducting gravity gradiometer have been demonstrated by Paik *et al.*¹² Error models were analyzed by Wang.¹³ Mapoles¹⁴ has extended the development of a displacement-differencing gravity gradiometer. In this work we have chosen the current-differencing scheme. One advantageous feature of the current-differencing gradiometer is the remote coupling of the two differencing acceleration transducers independent of their separation and their respective orientations. Therefore, three in-line (or diagonal) component gradiometers can be combined together by mounting all three pairs of acceleration transducers on the six faces of a common cube, with the sensitive axes normal to the surfaces of the cube, to form a three-axis in-line component gravity gradiometer. Construction of cross- (or off-diagonal) component gravity gradiometer is feasible by orienting the sensitive axes of the acceleration transducers perpendicular to the direction of the baseline. A tensor gravity gradiometer to measure all the six Γ_{ij} components has been proposed¹⁵ as a combination of the in-line and cross-component gradiometers.

While developing a three-axis gradiometer for precision gravity experiments in Earth's orbit,¹⁶ we have completed, with our colleague, a prototype single-axis in-line component gradiometer. This instrument has been used to perform a laboratory null test of the gravitational inverse-square law.¹⁷ The details of this gradiometer

development are described in Ref. 18 in which the theory of the gradiometer has been given a new formulation with generalization and more rigor than the preliminary analysis in Ref. 13. This paper (I) is a modified version of this new theoretical analysis with an extended error model of the instrument. Paper II presents the construction and test results of the gradiometer. Although we confine ourselves to the discussion of an in-line component gradiometer with a particular superconducting circuit chosen, the methods developed in these papers could easily be adapted to cross-component gradiometers and different superconducting circuits.

II. PRINCIPLE OF GRAVITY GRADIENT DETECTION

In this section we briefly review the basic principle of separating the gravity signal from dynamical variables and set a basis for the error model developed in Sec. V. Let the instrument platform be moving with respect to an inertial frame with an instantaneous angular velocity $\Omega(t)$ and linear acceleration $\mathbf{a}(t)$. Then, the accelerations of a proof mass observed in the two coordinate systems are related by the well-known equation¹⁹

$$\left(\frac{d^2 \mathbf{r}}{dt^2} \right)_{\text{in}} = \left(\frac{d^2 \mathbf{r}}{dt^2} \right)_{\text{pl}} + \Omega \times (\Omega \times \mathbf{r}) + 2\Omega \times \left(\frac{d\mathbf{r}}{dt} \right)_{\text{pl}} + \left(\frac{d\Omega}{dt} \right)_{\text{pl}} \times \mathbf{r} + \mathbf{a}. \quad (3)$$

Here the subscripts in and pl represent the inertial and platform coordinate systems in which respective measurements are made. The second and third terms on the right-hand side are the centrifugal and the Coriolis accelerations, respectively. If $\phi(\mathbf{r}, t)$ is the gravitational potential in the inertial frame, the resulting acceleration of the proof mass with respect to the moving platform is given by

$$\begin{aligned} \mathbf{g}'(\mathbf{r}, t) &\equiv \left(\frac{d^2 \mathbf{r}}{dt^2} \right)_{\text{pl}} \\ &= -\nabla \phi(\mathbf{r}, t) - \Omega \times (\Omega \times \mathbf{r}) \\ &\quad - 2\Omega \times \left(\frac{d\mathbf{r}}{dt} \right)_{\text{pl}} - \left(\frac{d\Omega}{dt} \right)_{\text{pl}} \times \mathbf{r} - \mathbf{a}(t). \end{aligned} \quad (4)$$

The Coriolis term produces a force perpendicular to the velocity in the platform coordinates and therefore drops out when the proof mass is confined to move in a single direction. The quantity $\mathbf{g}'(\mathbf{r}, t)$ is what is measured by an accelerometer or a gravimeter undergoing an acceleration.

It is clear from Eq. (4) that the *linear* acceleration term $-\mathbf{a}(t)$ can be eliminated by a differential measurement over a spatial coordinate x_j :

$$\begin{aligned} \frac{\partial g'_i(\mathbf{r}, t)}{\partial x_j} &= -\frac{\partial^2 \phi(\mathbf{r}, t)}{\partial x_i \partial x_j} - \frac{\partial}{\partial x_j} [\Omega_i (\Omega \cdot \mathbf{r}) - \Omega^2 x_i] \\ &\quad - \sum_{k,l} \epsilon_{ikl} \left(\frac{d\Omega_k}{dt} \right)_{\text{pl}} \frac{\partial x_l}{\partial x_j}. \end{aligned} \quad (5)$$

Substituting $\partial x_i / \partial x_j = \delta_{ij}$, and introducing the notations of Eq. (1) and

$$\Gamma'_{ij}(\mathbf{r}, t) \equiv \frac{\partial'_i(\mathbf{r}, t)}{\partial x_j}, \quad (6)$$

$$\alpha_k(t) \equiv \left[\frac{d\Omega_k}{dt} \right]_{pl}, \quad (7)$$

one finds

$$\Gamma'_{ij}(\mathbf{r}, t) = \Gamma_{ij}(\mathbf{r}, t) - (\Omega_i \Omega_j - \Omega^2 \delta_{ij}) + \sum_k \epsilon_{ijk} \alpha_k(t). \quad (8)$$

Notice that the *angular* acceleration term is antisymmetric whereas the first two terms in Eq. (8) are symmetric tensors. Therefore, one can further drop $\alpha(t)$ by symmetrization of Γ'_{ij} :

$$\begin{aligned} \Gamma'_{(ij)}(\mathbf{r}, t) &\equiv \frac{1}{2} \left[\frac{\partial g'_i}{\partial x_j} + \frac{\partial g'_j}{\partial x_i} \right] \\ &= \Gamma_{ij}(\mathbf{r}, t) - (\Omega_i \Omega_j - \Omega^2 \delta_{ij}). \end{aligned} \quad (9)$$

The centrifugal acceleration term can be taken out in principle by taking another spatial derivative: i.e., by means of a third-order gravity gradiometer. In practice, one measures Ω with the aid of gyroscopes and removes the effect of the centrifugal acceleration by actively stabilizing the platform or by compensating the induced error.

The *diagonal* component of the tensor, $\Gamma'_{(ii)} = \Gamma'_{ii}$, can be measured by detecting the relative acceleration along the in-line direction between *two* proof masses, separated in the x_i direction. The *off-diagonal* components $\Gamma'_{(ij)}$ ($j \neq i$), however, requires *four* proof masses because of the symmetrization. The relative accelerations in the cross sections in two pairs of accelerometers, which are separated in the x_i and x_j directions, respectively, can be added to yield $\Gamma'_{(ij)}$. Notice that one can instead subtract these two signals to determine the antisymmetric component:

$$\Gamma'_{[ij]}(\mathbf{r}, t) \equiv \frac{1}{2} \left[\frac{\partial g'_i}{\partial x_j} - \frac{\partial g'_j}{\partial x_i} \right] = \sum_k \epsilon_{ijk} \alpha_k(t). \quad (10)$$

The angular acceleration of the platform can be obtained by inverting this equation:

$$\alpha_k(t) = \epsilon_{ijk} \Gamma'_{[ij]}(\mathbf{r}, t). \quad (11)$$

A time integration of this vector then gives an alternative means of determining the angular velocity Ω .

A *tensor* gravity gradiometer with common mode readouts is therefore self-sufficient for true gravity detection.¹⁵ On the other hand, the device can measure true linear and angular accelerations of a moving platform by removing gravity-induced errors. Equation (4) shows that the gravitational field $-\nabla\phi$ remains as the fundamental error in linear acceleration measurement after removing dynamical error terms. The gravity gradiometer comes to the rescue. The gradient output $\vec{\Gamma}$ can be integrated over a spatial coordinate to determine $-\nabla\phi$. Therefore, a true accelerometer requires an aid from a gradiometer.

The symmetrization technique discussed above has been incorporated in the rotating gravity gradiometers^{6,7} whereas, in the floated gradiometer which has only two proof masses,⁸ the angular motion of the gradiometer is attenuated by floating the proof masses in a liquid. In the rotating gradiometers, the common mode acceleration \mathbf{g}' is further rejected by its frequency characteristic. The gradient $\vec{\Gamma}$, being a tensor of rank 2, is modulated at the second harmonic of the rotation frequency whereas the acceleration \mathbf{g}' is modulated at the fundamental frequency by its vector nature.⁶ A side benefit of this heterodyne detection is the translation of signal bandwidth away from the $1/f$ noise region of the instrument in frequency space. The mechanical rotation, however, brings in a penalty: additional, dynamically induced errors. From Eq. (8) one can clearly see, for example, the devastating effect of the angular velocity error $\delta\Omega$, which now contributes a first-order term $O(\Omega\delta\Omega)$ to the measurement.

For the prototype superconducting gravity gradiometer, we have chosen a nonrotating configuration. The extreme stability of the superconducting sensing circuit, combined with the low noise of the SQUID amplifier down to low signal frequencies, permits a very high degree of common mode rejection without rotation. For orbital applications, however, the superconducting gradiometer could be rotated to its advantage by spinning the entire satellite quietly.

The symmetric nature of Γ_{ij} has been used to construct a gravity gradiometer. Further, the trace of this tensor is constrained by the Poisson equation:

$$\sum_i \Gamma_{ii}(\mathbf{r}, t) = -\nabla^2 \phi(\mathbf{r}, t) = -4\pi G \rho(\mathbf{r}, t), \quad (12)$$

which is a consequence of the inverse square law of the gravitational force. This leaves *five* independent components for the gravity gradient tensor Γ_{ij} . With a three-axis diagonal component gravity gradiometer, the validity of Eq. (12) could be tested by summing the three outputs and comparing the result with the local mass density ρ . This experiment has been proposed as a precision null test of the inverse square law²⁰ and an early result of such an experiment has been reported.¹⁷ In an actual experiment, the measured quantity is the trace of $\Gamma'_{(ij)}$:

$$\sum_i \Gamma'_{(ii)}(\mathbf{r}, t) = -4\pi G \rho(\mathbf{r}, t) + 2\Omega^2(t). \quad (13)$$

It is therefore important to suppress or separate out the centrifugal acceleration term carefully in such an experiment.

III. DYNAMICS OF THE SUPERCONDUCTING GRAVITY GRADIOMETER

The superconducting gravity gradiometer consists of a pair of superconducting acceleration transducers and a superconducting inductive load which is connected to a SQUID amplifier. The coupling between the transducers and the output load is provided by flux quantization.

The principle of one acceleration transducer element is first discussed and its equation of motion is then derived. Each transducer communicates to the rest of the superconducting circuit only through *one* current component

that flows through the transducer. In a coupled circuit of a pair of transducers and a load, flux quantization imposes constraints to the superconducting circuit. For detection purposes, the *currents at the load*, rather than the current through the transducers, are the observable quantities at the output. The complete dynamical equations are then linearized and expressed in terms of these currents, the respective displacements of the proof masses, together with the applied common and differential acceleration signals.²¹ Because the gradiometer is a differential accelerometer over a finite baseline, the gradiometer must reject common acceleration signals. The conditions for a common mode balance is derived. The parameters used to accomplish the balance are the persistent, but adjustable, currents stored in various superconducting loops. Further, a *wideband* common mode balance is shown to be possible by iteratively adjusting at least two current components. After balancing the common accelerations, only differential acceleration will be detected at the load. The transfer function of an applied differential acceleration to the corresponding current output at the load is derived.

Throughout the remainder of this paper, a variable with time or frequency dependency will be written explicitly as such functions, whereas the average values of these variables will be denoted by the same notation as the function, but with the functional dependency deleted.

A. Principle of a superconducting acceleration transducer

The principle of the superconducting acceleration transducer is illustrated schematically in Fig. 1. Analysis of this device as a resonant transducer for a gravitational-wave antenna and as a sensitive accelerometer has been given previously in a different format.⁹ A superconducting proof mass, which is suspended by spring and is confined to one linear degree of freedom, responds to an acceleration signal with a displacement relative to sensing coil. The inductance of the coil is then modulated, due to the Meissner effect, by the superconducting plane of the proof mass. The coil is connected to an output inductor through a superconducting path and a quantized magnetic flux is stored in the superconducting loop formed by the sensing and output inductors. The current flow through the output inductor is modulated as a result of the induc-

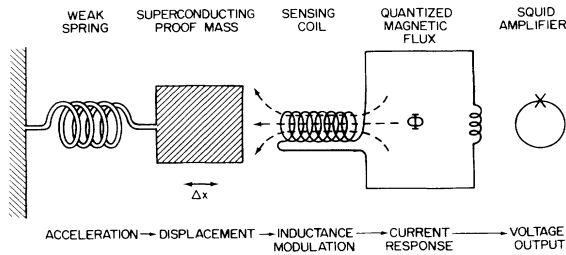


FIG. 1. Principle of the superconducting acceleration transducer.

tance modulation of the sensing coil. The persistent current provides the stability of the transducer scale factor. A low-noise SQUID amplifier is then used as a dc current-to-voltage power amplifier to produce a readout.

B. Analysis of a single acceleration transducer

The transfer of mechanical energy to electrical energy is accomplished at the sensing coil. In order that the sensing coil converts a displacement to a current more *linearly* within a transducer, a symmetrical pair of “pancake” coils are utilized. The coils are located on the opposite faces of the proof mass and are connected in parallel (Fig. 2). Each having winding density n_L and area A_L , the coils are at mean distances of d_a and d_b from the respective superconducting planes of the proof mass. If the displacement of the proof mass from its average position is $x(t)$, the inductances of the coils are given by

$$L_a(t) = \Lambda[d_a + x(t)] = L_a + \Lambda x(t), \tag{14a}$$

$$L_b(t) = \Lambda[d_b - x(t)] = L_b - \Lambda x(t). \tag{14b}$$

Here

$$\Lambda \equiv \mu_0 n_L^2 A_L, \tag{15}$$

where μ_0 is the permeability in free space and

$$L_a \equiv \langle L_a(t) \rangle, \quad L_b \equiv \langle L_b(t) \rangle, \tag{16}$$

as was noted earlier concerning notation.

Two current components are needed to characterize the electromagnetic state of the two sensing coils. One obvious choice of variables^{9,13} are the currents $I_a(t)$ and $I_b(t)$ which flow through each of the two coils, so that the electromagnetic energy in the two coils is

$$V_{EM} = \frac{1}{2} L_a(t) I_a(t)^2 + \frac{1}{2} L_b(t) I_b(t)^2. \tag{17}$$

However, in order to make the analysis simpler, a different choice¹⁸ of the two current variables can be made with the aim that the expression for the electromagnetic energy has as simple a denominator as possible. Such a way of choosing variables is a classical analog of the re-normalization procedure in quantum field theory.

Before making the choice, we make two observations. The first observation is that the series inductance of the sensing coils is a constant:⁹

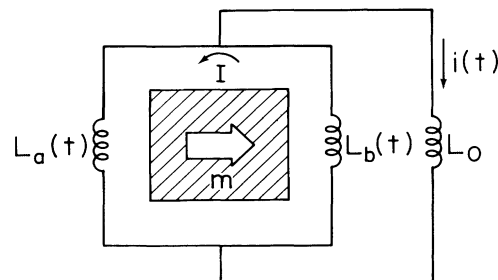


FIG. 2. Superconducting circuit and its current variables of a single acceleration transducer.

$$L_s(t) \equiv L_a(t) + L_b(t) = L_a + L_b = L_s . \quad (18)$$

Consequently, the current I through the superconducting loop of these two inductors in series is also a constant because the trapped flux Φ_{ab} in this loop is quantized. The second observation is that the parallel combination of the two sensing coils has a constant denominator in the expression for its inductance:

$$\begin{aligned} L_p(t) &\equiv \frac{L_a(t)L_b(t)}{L_a(t) + L_b(t)} \\ &= \frac{1}{L_a + L_b} [L_a L_b - (L_a - L_b)\Lambda x(t) - \Lambda^2 x^2(t)] . \end{aligned} \quad (19)$$

In fact, even the numerator of this parallel inductance will also be a constant up to the first order if the mean spacings d_a and d_b are matched so as to make $L_a \simeq L_b$. The nonlinearity of the inductance modulation is exhibited by the second-order term in Eq. (19).

Expressed in terms of one parameter Φ_{ab} and one current variable $i(t)$, which flows through the parallel combination of $L_a(t)$ and $L_b(t)$, the electromagnetic energy has a *constant denominator* and has thus acquired a “renormalized” form:

$$V_{EM} = \frac{1}{2} \frac{\Phi_{ab}^2}{L_a + L_b} + \frac{1}{2} L_p(t) i^2(t) . \quad (20)$$

It is straightforward to show that the expressions in Eqs. (17) and (20) are equivalent to each other.¹⁸

The only variable $i(t)$, once the parameter I or Φ_{ab} is fixed, possesses *all* the dynamical information in the electromagnetic system of the transducer. As the inductances $L_a(t)$ and $L_b(t)$ are modulated by the displacement of the proof mass, the current $i(t)$ must always split between the two inductors according to the inverse ratio of the respective inductances in order to produce equal and opposite magnetic flux contributions to the superconducting loop formed by the series inductor $L_a + L_b$. The net currents $I_a(t)$ and $I_b(t)$ through $L_a(t)$ and $L_b(t)$ are therefore the following linear combinations of I and $i(t)$:

$$I_a(t) = \frac{L_b(t)}{L_a + L_b} i(t) - I , \quad (21a)$$

$$I_b(t) = \frac{L_a(t)}{L_a + L_b} i(t) + I . \quad (21b)$$

The force due to magnetic field pressure on the proof mass is given by

$$\begin{aligned} F_{EM} &= - \frac{\partial}{\partial x} \left[\frac{\Phi_a^2(t)}{2L_a(t)} + \frac{\Phi_b^2(t)}{2L_b(t)} \right] \Big|_{\Phi_a, \Phi_b} \\ &= \frac{\Lambda}{2} [I_a^2(t) - I_b^2(t)] , \end{aligned} \quad (22)$$

where $\Phi_a(t)$ and $\Phi_b(t)$ denote magnetic fluxes in $L_a(t)$ and $L_b(t)$, respectively. In terms of I and $i(t)$, this force can be rewritten as

$$F_{EM} = -\Lambda \left[I + \frac{1}{2} \frac{L_a(t) - L_b(t)}{L_a + L_b} i(t) \right] i(t) . \quad (23)$$

The total force acting on the proof mass consists of this magnetic force together with a restoring force of the mechanical spring suspension of the proof mass and any externally applied force $f(t)$ on the proof mass relative to the platform of the sensing coils. We will ignore the effects of the damping term for the time being. When the proof mass m is approximated as a point mass located at its center of mass \mathbf{r} , the external force becomes

$$f(t) = m \hat{\mathbf{n}} \cdot \mathbf{g}'(\mathbf{r}, t) , \quad (24)$$

where $\hat{\mathbf{n}}$ is the unit vector along the direction of the sensitive axis and $\mathbf{g}'(\mathbf{r}, t)$ is the specific force given by Eq. (4). The equation of motion for the proof mass in the platform frame can now be written as

$$\begin{aligned} \ddot{x}'(t) + \omega_M^2 x'(t) + \frac{\Lambda}{m} \left[I + \frac{1}{2} \frac{L_a(t) - L_b(t)}{L_a + L_b} i(t) \right] i(t) \\ = \hat{\mathbf{n}} \cdot \mathbf{g}'(\mathbf{r}, t) , \end{aligned} \quad (25)$$

where ω_M is the angular resonance frequency of the mechanical spring. An alternative derivation of this equation, in which an electromechanical Lagrangian approach is used for the superconducting transducer, is found in Ref. 18.

The dc component of Eq. (25) defines the equilibrium position x_0 of the proof mass. This position is shifted from the relaxed position of the mechanical spring by Earth's gravity \mathbf{g}_E and by a dc magnetic force. Substituting

$$x'(t) \equiv x_0 + x(t) , \quad (26a)$$

$$\mathbf{g}'(\mathbf{r}, t) \equiv \mathbf{g}_E(\mathbf{r}) + \mathbf{g}_P(\mathbf{r}, t) , \quad (26b)$$

into Eq. (25), we find

$$x_0 = - \frac{g_E \cos \theta_n}{\omega_M^2} \frac{\Lambda}{m \omega_M^2} \left[I + \frac{1}{2} \frac{L_a - L_b}{L_a + L_b} i \right] i , \quad (27)$$

in the general case where $i \equiv \langle i(t) \rangle \neq 0$. Here θ_n is the angle that the sensitive axis makes with the upward vertical. The local vertical is defined by Earth's gravity vector which is found from Eq. (4) as

$$\mathbf{g}_E(\mathbf{r}) = -\nabla \phi_E(\mathbf{r}) - \boldsymbol{\Omega}_E \times [\boldsymbol{\Omega}_E \times (\mathbf{R}_E + \mathbf{r})] , \quad (28)$$

where $\phi_E(\mathbf{r})$, $\boldsymbol{\Omega}_E$, and \mathbf{R}_E are, respectively, Earth's gravitational potential, spin angular velocity, and the geocentric position vector of the coordinate origin.

The *linearized* equation of motion for the ac part, after Fourier transformation, can be readily shown as

$$\left[-\omega^2 + \omega_M^2 + \frac{\Lambda^2 i^2}{m L_s} \right] x(\omega) + \frac{\Lambda I'}{m} i(\omega) = g(\omega) , \quad (29)$$

where $g(\omega)$ is the Fourier transform of

$$g(t) \equiv \hat{\mathbf{n}} \cdot \mathbf{g}_P(\mathbf{r}, t) \quad (30)$$

and

$$I' \equiv I + \frac{L_a + L_b}{L_a + L_b} i. \quad (31)$$

There are two independent superconducting loops in the circuit. The flux quantization condition in the loop $L_a(t) + L_b(t)$ has already been used in representing I as a constant. An additional constraint in the dynamical equation comes from the flux quantization condition in the loop $L_b(t) + L_0$:

$$L_b(t)I_b(t) + L_0 i(t) = \Phi_{b0}. \quad (32)$$

The *first-order* equation becomes, after Fourier transformation,

$$\Lambda I' x(\omega) = (L_0 + L_p) i(\omega). \quad (33)$$

Simultaneous equations (29) and (33) determine the dynamics of a single transducer completely. In particular, the acceleration-to-current transfer function can be shown to be

$$H_{gi}(\omega) = \frac{1}{\omega_0^2 - \omega^2} \frac{\Lambda I'}{L_0 + L_p}. \quad (34)$$

Here, ω_0 is the resulting angular resonance frequency of the transducer due to the addition of spring constant $m\omega_M^2$ by the superconducting circuit:

$$\omega_0^2 \equiv \omega_M^2 + \frac{\Lambda^2 i^2}{mL_s} + \frac{\Lambda^2 I'^2}{m(L_0 + L_p)}. \quad (35)$$

C. Dynamical equations for the gradiometer

The gradiometer, shown in Fig. 3, consists of a pair of the above acceleration transducers and a superconducting inductive load. The coupling among these elements is through flux quantization in the superconducting circuit which has four independent superconducting loops.

The dynamical equations for each transducer is analogous to Eqs. (29) and (33) for a single accelerometer. An additional subscript

$$k = 1 \text{ or } 2 \quad (36)$$

is now used for the respective variables and parameters to distinguish between the two transducers. With this subscript, the *linearized* equations of motion for the proof masses in the transducers, being similar to Eq. (29), are written as

$$\left[-\omega^2 + \omega_{kM}^2 + \frac{\Lambda^2 i_k^2}{m_k L_{ks}} \right] x_k(\omega) + \frac{\Lambda I'_k}{m_k} i_k(\omega) = g_k(\omega). \quad (37)$$

Here the geometries of the sensing coils are again assumed to be identical so that they can be represented by a single

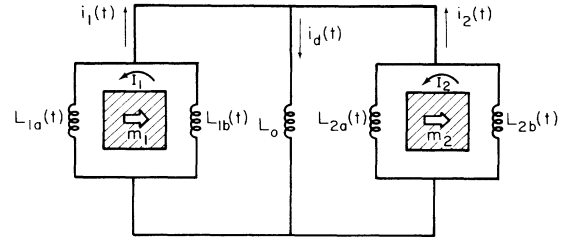


FIG. 3. Superconducting circuit of the current-differencing gradiometer.

parameter Λ defined by Eq. (15). Also, the two flux quantization constraints in the superconducting loops $L_{ka} + L_{kb}$ have again been used in deriving Eq. (37). Two more constraints, similar to Eq. (33), are obtained by using flux quantization conditions in two other independent superconducting loops such as $L_{kb}(t) + L_0$. However, a generalization from Eq. (33) is needed here because the current through L_0 is now the sum of the current outputs from each transducer. The *linearized* constraints are therefore given by

$$\Lambda I'_k x_k(\omega) = L_{kp} i_k(\omega) + L_0 [i_1(\omega) + i_2(\omega)]. \quad (38)$$

Notice that these two equations are coupled through $i_1(\omega)$ and $i_2(\omega)$.

The dynamics of the gradiometer, governed by the four coupled equations (37) and (38) in the four variables $x_k(\omega)$ and $i_k(\omega)$, has 2 degrees of freedom. Each of the two transducers couple to the rest of the circuit through *one single current* signal: $i_1(\omega)$ or $i_2(\omega)$. Depending on the signature of the applied acceleration components, these current modulations can add or subtract at the output inductor L_0 . It is therefore convenient to use a new set of current variables $i_d(\omega)$ and $i_c(\omega)$ defined by the sum and half of the difference of the two transducer currents. In terms of $i_d(\omega)$ and $i_c(\omega)$, the transducer currents $i_1(\omega)$ and $i_2(\omega)$ can be expressed as

$$i_k(\omega) = \frac{1}{2} i_d(\omega) + (-1)^k i_c(\omega). \quad (39)$$

Likewise, the applied accelerations $g_1(t)$ and $g_2(t)$ at the proof masses m_1 and m_2 can be expressed in terms of their *differential* and *common accelerations*, $g_d(\omega)$ and $g_c(\omega)$, as

$$g_k(\omega) = (-1)^k \frac{1}{2} g_d(\omega) + g_c(\omega). \quad (40)$$

Notice that $i_d(\omega)$ is the actual current flowing through L_0 and detected by the SQUID.

With the change of variables in Eqs. (39) and (40), the dynamical equations (37) and (38) become

$$\left[-\omega^2 + \omega_{kM}^2 + \frac{\Lambda^2 i_k^2}{m_k L_{ks}} \right] x_k(\omega) + \frac{\Lambda I'_k}{m_k} \frac{1}{2} i_d(\omega) + (-1)^k \frac{\Lambda I'_k}{m_k} i_c(\omega) = (-1)^k \frac{1}{2} g_d(\omega) + g_c(\omega), \quad (41)$$

$$x_k(\omega) = \frac{L_{kp} + 2L_0}{\Lambda I'_k} \frac{1}{2} i_d(\omega) + (-1)^k \frac{L_{kp}}{\Lambda I'_k} i_c(\omega). \quad (42)$$

Upon eliminating the displacement coordinates we obtain

$$(-\omega^2 + \omega_{kd}^2) \frac{L_{kp} + 2L_0}{\Lambda I'_k} \frac{1}{2} i_d(\omega) + (-1)^k (-\omega^2 + \omega_{kc}^2) \frac{L_{kp}}{\Lambda I'_k} i_c(\omega) = (-1)^k \frac{1}{2} g_d(\omega) + g_c(\omega) = g_k(\omega), \quad (43)$$

where

$$\omega_{kc}^2 \equiv \omega_{kM}^2 + \frac{1}{m_k} \left[\frac{\Lambda^2 i_k^2}{L_{ks}} + \frac{\Lambda^2 I_k'^2}{L_{kp}} \right], \quad (44a)$$

$$\omega_{kd}^2 \equiv \omega_{kM}^2 + \frac{1}{m_k} \left[\frac{\Lambda^2 i_k^2}{L_{ks}} + \frac{\Lambda^2 I_k'^2}{L_{kp} + 2L_0} \right]. \quad (44b)$$

Solving Eq. (43) for the signal current we find

$$i_d(\omega) = H_{gi}^d(\omega) g_d(\omega) + H_{gi}^c(\omega) g_c(\omega), \quad (45)$$

where $H_{gi}^d(\omega)$ and $H_{gi}^c(\omega)$ are the transfer functions from $g_d(\omega)$ and $g_c(\omega)$, respectively, to $i_d(\omega)$. These transfer functions of the gradiometer are given by

$$H_{gi}^d(\omega) = \frac{\frac{1}{\omega_{2c}^2 - \omega^2} \frac{\Lambda I'_2}{L_{2p}} + \frac{1}{\omega_{1c}^2 - \omega^2} \frac{-\Lambda I'_1}{L_{1p}}}{\frac{\omega_{2d}^2 - \omega^2}{\omega_{2c}^2 - \omega^2} \frac{2L_0 + L_{2p}}{L_{2p}} + \frac{\omega_{1d}^2 - \omega^2}{\omega_{1c}^2 - \omega^2} \frac{2L_0 + L_{1p}}{L_{1p}}}, \quad (46a)$$

$$H_{gi}^c(\omega) = \frac{2 \left[\frac{1}{\omega_{2c}^2 - \omega^2} \frac{\Lambda I'_2}{L_{2p}} - \frac{1}{\omega_{1c}^2 - \omega^2} \frac{-\Lambda I'_1}{L_{1p}} \right]}{\frac{\omega_{2d}^2 - \omega^2}{\omega_{2c}^2 - \omega^2} \frac{2L_0 + L_{2p}}{L_{2p}} + \frac{\omega_{1d}^2 - \omega^2}{\omega_{1c}^2 - \omega^2} \frac{2L_0 + L_{1p}}{L_{1p}}}. \quad (46b)$$

The four parameters ω_{kd} and ω_{kc} are, in general, not the two resonances of the gradiometer. Nevertheless, comparing the expressions for these parameters with Eqs. (34) and (35) suggests intuitive meaning to these nonobservable. Thus, ω_{kc} can represent the angular resonance frequencies that the two transducers would separately have if they were each connected to a short-circuited load. A short-circuited load arises in these models because, when $i_d(\omega) = 0$ in the gradiometer circuit, the two transducers are driving the current $i_c(\omega)$ in a push-pull manner, contributing zero impedance to each other. Likewise, ω_{kd} can represent the angular resonance frequencies that the two transducers would separately have if they were each loaded with an inductance of $2L_0$ but were otherwise decoupled from each other. The appearance of $2L_0$ here is due to the equal contributions of currents $\frac{1}{2} i_d(\omega)$ to the signal at L_0 . Thus, under the restriction $i_c(\omega) = 0$, the flux modulation produced by each transducer at L_0 as seen by the transducer itself is doubled by the presence of the other transducer. The transfer functions

of these separated model accelerators are given from Eq. (43) as

$$\left. \frac{\partial i_d}{\partial g_k} \right|_{i_c} = \frac{(-1)^k \Lambda I'_k}{2L_0 + L_{kp}} \frac{1}{\omega_{kd}^2 - \omega^2}, \quad (47a)$$

$$\left. \frac{\partial i_c}{\partial g_k} \right|_{i_d} = \frac{(-1)^k \Lambda I'_k}{L_{kp}} \frac{1}{\omega_{kc}^2 - \omega^2}. \quad (47b)$$

D. Common mode balance and gradiometer transfer function

For operation as a gradiometer in the presence of common accelerations, the transducers need to be tuned such that $H_{gi}^c(\omega) = 0$. No common acceleration signal will then appear at the output load L_0 , and the coupled acceleration transducers are said to operate in a "gradiometer mode." On the other hand, parameters can be chosen such that $H_{gi}^d(\omega)$ vanishes instead. Then, the output will respond only to common accelerations and the system is said to operate in an "accelerometer mode." The accelerometer mode operation is a powerful means of obtaining a precise calibration of the gradiometer. A detailed discussion of the accelerometer mode is found in Sec. IV B of paper II. From Eq. (46b) the *common mode balance* is obtained when

$$\frac{-\Lambda I'_1}{(\omega_{1c}^2 - \omega^2) L_{1p}} = \frac{\Lambda I'_2}{(\omega_{2c}^2 - \omega^2) L_{2p}}. \quad (48)$$

This balance condition can be satisfied at any single frequency by adjusting only one persistent current parameter. Balancing over a small frequency range near dc appears sufficient for normal low-frequency use of the gradiometer in which $\omega \ll \omega_{1c}, \omega_{2c}$. In the terrestrial environment, however, the environmental vibrations occur in a wideband and are very large compared with the extremely weak gravitational signals. A *wideband* balance will help to immunize the gradiometer against such environmental vibrations.

The four current components I_1, I_2, i_1 , and i_2 , do provide more than sufficient degrees of freedom to tune for wideband balance. In principle, Eq. (48) becomes an identity if

$$\omega_{1c} = \omega_{2c} \quad (49a)$$

and

$$\frac{-\Lambda I'_1}{L_{1p}} = \frac{\Lambda I'_2}{L_{2p}} \quad (49b)$$

are simultaneously satisfied. However, direct matching of ω_{kc} is not practical because these equivalent resonances

are observable only when the output load is shorted and when the two transducers are also decoupled mechanically.¹⁸ In the experiment, a wideband balance can be achieved instead by iterating the balance at two frequencies. Tuning I_1 or I_2 to balance out an applied common acceleration at a high frequency ($\omega \gg \omega_{1c}, \omega_{2c}$) will achieve the condition (49b). This adjustment is followed by tuning of i_1 or i_2 for balance at a low frequency ($\omega \ll \omega_{1c}, \omega_{2c}$), yielding

$$-\frac{1}{\omega_{1c}^2} \frac{\Delta I'_1}{L_{1p}} = \frac{1}{\omega_{2c}^2} \frac{\Delta I'_2}{L_{2p}}. \quad (49c)$$

The latter operation will, in general, affect the previous balance (49b), and iteration between the two balance procedures is needed. When the conditions (49b) and (49c) are both satisfied, condition (49a) follows. This frequency-independent balance has been applied in the experiment and is reported in paper II.

Upon substitution of Eq. (48) into Eq. (46a), $H_{gi}^d(\omega)$ assumes a simple form:

$$[H_{gi}^d(\omega)]^{-1} = (\omega_{1d}^2 - \omega^2) \frac{L_0 + \frac{1}{2}L_{1p}}{-\Delta I'_1} + (\omega_{2d}^2 - \omega^2) \frac{L_0 + \frac{1}{2}L_{2p}}{\Delta I'_2}. \quad (50)$$

Notice that the transfer function of a balanced gradiometer becomes the harmonic mean of the transfer functions of the two separated model accelerometers, given by Eq. (47a).

When the common mode balance is not precise, $H_{gi}^c(\omega) \neq 0$ constitutes an error coefficient. This error, which will be discussed in Sec. V, is obtained from Eqs. (46) as

$$H_{gi}^c(\omega) \simeq H_{gi}^d(\omega) \frac{\frac{1}{\omega_{2c}^2 - \omega^2} \frac{\Delta I'_2}{L_{2p}} - \frac{1}{\omega_{1c}^2 - \omega^2} \frac{-\Delta I'_1}{L_{1p}}}{\frac{1}{2} \left[\frac{1}{\omega_{2c}^2 - \omega^2} \frac{\Delta I'_2}{L_{2p}} + \frac{1}{\omega_{1c}^2 - \omega^2} \frac{-\Delta I'_1}{L_{1p}} \right]}. \quad (51)$$

In the foregoing analysis, the transducer has been approximated as a linear system. The dynamical equations (25) and (32), however, are *nonlinear* in nature so that the response current $i_d(\omega)$ must contain nonlinear terms in general, in addition to the linear terms shown in Eq. (45). These nonlinear terms may not drop out even when $H_{gi}^c(\omega) = 0$. The scale factor nonlinearity therefore constitutes an important error source, which will be discussed in Sec. V of this paper and in Appendix B of paper II.

E. Equivalent accelerometer representation

With two coupled acceleration transducers in the gradiometer, only the differential acceleration is the measured signal at L_0 . The common acceleration drops out upon balance. Therefore, a convenient representation of the gradiometer is a single (differential) accelerometer which converts a differential acceleration into a signal

current. Such a representation involves identification of the gradiometer transfer function with the parameters of a *single accelerometer*, as discussed in Sec. III B. These parameters include a resonance frequency, a mass, and the parameters of a superconducting circuit.

The two normal mode resonance frequencies of the gradiometer are some weighted average of the parameters ω_{1c} and ω_{2c} for the common mode and also some other weighted average of ω_{1d} and ω_{2d} for the differential mode. In the particular case of wideband balance, ω_{1c} and ω_{2c} are equal to each other and hence equal to the common mode angular resonance frequency, denoted by ω_c . The differential mode angular resonance frequency, denoted by ω_0 , is then defined from the singularity of $H_{gi}^d(\omega)$ in Eq. (50). In practice, the gradiometer need only be balanced at a limited frequency band of the signal. Then Eq. (50) is only valid in this limited frequency band. Therefore, the exact differential mode resonance is determined from the singularity of $H_{gi}^d(\omega)$ in the more general equation (46a). Yet, as far as signal transduction within the limited signal frequency band is concerned, we can still use Eq. (50) to define ω_0 .

By defining equivalent circuit parameters to satisfy

$$\frac{L_0 + L_p}{I'} \equiv \frac{L_0 + \frac{1}{2}L_{1p}}{-I'_1} + \frac{L_0 + \frac{1}{2}L_{2p}}{I'_2}, \quad (52)$$

we can convert Eq. (50) into the form of Eq. (34):

$$H_{gi}^d(\omega) \equiv \frac{\Delta I'}{L_0 + L_p} \frac{1}{\omega_0^2 - \omega^2}, \quad (53)$$

where the effective resonance frequency ω_0 is related to ω_{kd}^2 by

$$\frac{L_0 + L_p}{I'} \omega_0^2 \equiv \frac{L_0 + \frac{1}{2}L_{1p}}{-I'_1} \omega_{1d}^2 + \frac{L_0 + \frac{1}{2}L_{2p}}{I'_2} \omega_{2d}^2. \quad (54)$$

While there is freedom in defining the individual circuit parameters which appear on the left-hand side of Eq. (52), one natural choice is to identify L_0 with the load inductance and L_p with the output inductance of the superconducting circuit:

$$\frac{1}{L_p} \equiv \frac{1}{L_{1p}} + \frac{1}{L_{2p}}. \quad (55)$$

Then, the current parameter I' is defined by Eq. (52). With the aid of Eqs. (49b) and (55), this definition of I' in Eq. (52) simplifies to

$$\frac{1}{I'} \equiv \frac{1}{-I'_1} + \frac{1}{I'_2}, \quad (56)$$

under wideband balance condition.

The transfer function in Eq. (53) has only characterized the overall signal transduction of the gradiometer. The intrinsic noise of the gradiometer will be given in Sec. IV in terms of Brownian motion noise and amplifier noise. For a single spring-mass system, the Brownian motion depends on the mass and the fluctuating force of the spring. Therefore, once the *effective mass* in the equivalent accelerometer representation is determined, the Brownian motion of the two coupled acceleration transducers in the

differential mode can be derived using this equivalent single spring-mass model. This effective mass requires a *unique* definition in order to give the correct Brownian motion noise of the gradiometer and must therefore be derived from the dynamics of the gradiometer.

Dynamically, the gradiometer consists of two coupled masses connected to the platform and to each other by three springs. Thus, the homogeneous equations of motion of the two proof masses are obtained by eliminating $i_k(\omega)$ from Eqs. (37) and (38):

$$\omega^2 m_k x_k(\omega) = K_k x_k(\omega) + K_{12} x_{3-k}(\omega), \quad (57)$$

where the three spring constants K_k and K_{12} are given by

$$K_k \equiv m_k \omega_{kM}^2 + \frac{\Lambda^2 i_k^2}{L_{ks}} + \frac{(\Lambda L'_k)^2 (L_0 + L_{kp})}{(L_0 + L_p)(L_{1p} + L_{2p})}, \quad (58)$$

$$K_{12} \equiv \frac{(-\Lambda I'_1)(\Lambda I'_2)L_0}{(L_0 + L_p)(L_{1p} + L_{2p})}. \quad (59)$$

Now, we need to find out what displacement variable, $x_d(\omega)$, causes the signal current $i_d(\omega)$. Thus, we break up the signal transduction into two intermediate steps: $g_d(\omega)$ to $x_d(\omega)$ and then $x_d(\omega)$ to $i_d(\omega)$. From Eqs. (41) and (42), we obtain

$$(-\omega^2 + \omega_0^2)x_d(\omega) = g_d(\omega), \quad (60)$$

$$i_d(\omega) = \frac{\Lambda I'}{L_0 + L_p} x_d(\omega), \quad (61)$$

where

$$x_d(\omega) \equiv \frac{L_p}{I'} \left[\frac{I'_2}{L_{2p}} x_2(\omega) - \frac{-I'_1}{L_{1p}} x_1(\omega) \right]. \quad (62)$$

The effective mass is therefore the inertia for the coupled spring-mass system of Eqs. (57)–(59) toward the motion $x_d(\omega)$ of Eq. (62).

We next note that a simple scaling of the two separate displacement variables,

$$x'_k(\omega) \equiv \frac{L_p}{I'} \frac{(-1)^k I'_k}{L_{kp}} x_k(\omega), \quad (63)$$

simplifies $x_d(\omega)$ into the form

$$x_d(\omega) \equiv x'_2(\omega) - x'_1(\omega). \quad (64)$$

The corresponding scaling required for the masses and spring constants are

$$m'_k \equiv \left[\frac{x_k}{x'_k} \right]^2 m_k, \quad (65a)$$

$$K'_k \equiv \left[\frac{x_k}{x'_k} \right]^2 K_k, \quad (65b)$$

$$K'_{12} \equiv \frac{x_1 x_2}{x'_1 x'_2} K_{12}, \quad (65c)$$

because, under these scaling, the dynamical equation (60) is invariant in form and both the kinetic and potential energies (within the frequency range of common mode balance) remain unchanged.

Now, the effective mass corresponding to $x_d(\omega)$ of Eq. (64) is just the reduced mass of m'_1 and m'_2 . By using Eqs. (63) and (65a), this effective mass, denoted by m , can be shown to satisfy a simple formula:

$$\frac{L_p^2}{I'^2 m} \equiv \frac{L_{1p}^2}{I_1'^2 m_1} + \frac{L_{2p}^2}{I_2'^2 m_2}. \quad (66)$$

In Sec. IV A the effective mass defined here will be used in conjunction with the equivalent accelerometer representation for finding the Brownian motion noise of the transducer.

IV. NOISE AND OPTIMIZATION

In the light of the equivalent accelerometer model given in Sec. III E, the fundamental noise terms of the gradiometer will be derived by treating the gradiometer as a single accelerometer. In this section we introduce damping and consider its effects.

A. Transducer Brownian motion noise

The fundamental noise source of a spring-mass system at a temperature T is the Brownian motion of the harmonic oscillator at that temperature. The force of the spring on the proof mass undergoes random fluctuations. The spectral density of such force fluctuations at the resonance frequency ω_0 of the oscillator is related, by the fluctuation-dissipation theorem, to the damping of the oscillator at resonance.

In applying the fluctuation-dissipation theorem, emphasis is made here that measurement of relaxation time $\tau(\omega_0)$ or quality factor $Q(\omega_0) \equiv \omega_0 \tau(\omega_0)$ gives information on the force fluctuations only at ω_0 . The Langevin equation is a modification of the equation of motion in Sec. III by including a damping term and an acceleration noise $g_n^T(\omega)$ term:

$$\left[-\omega^2 + \frac{j\omega}{\tau(\omega_0)} + \omega_0^2 \right] x(\omega) = g_n^T(\omega). \quad (67)$$

Thus the energy of the oscillator at a temperature T ,

$$m \omega_0^2 \langle x^2(t) \rangle = k_B T, \quad (68)$$

where

$$\langle x^2(t) \rangle = \int_0^\infty x(\omega) x^*(\omega) d\omega, \quad (69)$$

is dominated by its spectral density at resonance. Use of Eqs. (67)–(69) gives the Nyquist formula

$$S_g^T(\omega_0) = \frac{2}{\pi} k_B T \frac{1}{m \tau(\omega_0)}, \quad (70)$$

where $S_g^T(\omega_0)$ is the spectral density²² of the acceleration noise g_n^T at ω_0 .

The force or acceleration fluctuations at a signal frequency $\omega \ll \omega_0$ is in general *different* from that at ω_0 because the noise could have a complicated frequency dependence which is governed by the nature of the loss mechanisms in the spring. The noise at ω due to force fluctuations in the spring is obtained from Eq. (70) with $\tau(\omega_0)$ replaced by $\tau(\omega)$:

$$S_g^T(\omega) = \frac{2}{\pi} k_B T \frac{1}{m\tau(\omega)}. \quad (71)$$

A direct measurement of $\tau(\omega)$ requires shifting the resonance frequency from ω_0 to ω . In principle, one can increase the mass m or use a "negative spring"¹¹ so that the new spring-mass system indeed resonates at ω and therefore the Q factor of this new system can be measured. From a knowledge of the new mass used or of the loss in the negative spring, the dissipation in the original spring can be determined.

The Q factor of the accelerometer depends on both the mechanical and the electrical parameters because the electrochemical spring of the accelerometer has contributions from a mechanical spring and two electromagnetic springs, in the ratio given by the three terms in Eq. (35), for the total spring constant and hence for the stored ac energy at ω_0 . The power loss in each of these constituent springs is then proportional to this ratio of stored ac energies in these springs divided by a certain relaxation time at ω_0 . Therefore, the following relationship for the relaxation times results from the obvious observation that, at ω_0 , the total ac power loss is the sum of the power losses in the respective springs:

$$\frac{1}{\tau(\omega_0)} = \frac{1-\gamma-\beta}{\tau_M(\omega_0)} + \frac{\gamma}{\tau_i(\omega_0)} + \frac{\beta}{\tau_{I'}(\omega_0)}. \quad (72)$$

Here $\tau_M(\omega_0)$, $\tau_i(\omega_0)$, and $\tau_{I'}(\omega_0)$ are the relaxation times that each spring would have if it is separately resonated at ω_0 , and γ and β are the transducer coupling coefficients via i and I' defined by

$$\gamma \equiv \frac{\Lambda^2 i^2}{m\omega_0^2 L_s}, \quad (73a)$$

$$\beta \equiv \frac{\Lambda^2 I'^2}{m\omega_0^2 (L_0 + L_p)}. \quad (73b)$$

In order to reduce dissipation in all the constituent springs, choice of material and geometry, material treatment, surface preparation as well as choice of electrical parameters must be optimized.

B. SQUID amplifier noise

A SQUID can be modeled as an ideal current-to-voltage amplifier having an input inductor L_i and two noise generators for its voltage and current noise with spectral densities $S_V(\omega)$ and $S_I(\omega)$, respectively, at the amplifier input [see Fig. 4(a) and Ref. 23].

The optimum source impedance $(S_V/S_I)^{1/2}$ is much smaller than the parasitic impedance ωL_i unless L_i is tuned out (at one frequency) to noise match the input impedance. Therefore, when the SQUID is used as a wide-band amplifier, the noise is dominated by S_I and can be characterized by an "input energy sensitivity":

$$E_A(\omega) \equiv \frac{1}{2} L_i S_I(\omega). \quad (74)$$

In a practical gradiometer design, the transducer output inductance L_p is usually larger than L_i and a superconducting transformer is desired to bridge between L_p and L_i . The equivalent load, representing L_i and the

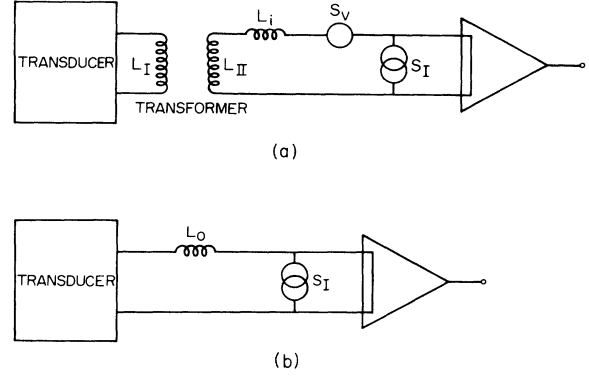


FIG. 4. (a) Transducer coupled to a SQUID through a transformer. (b) An equivalent circuit of the SQUID noise for an untuned SQUID input.

transformer, seen by the transducer is an inductor L_0 :

$$L_0 = \frac{L_i + (1 - k_t^2)L_{II}}{L_i + L_{II}} L_I, \quad (75)$$

where k_t , L_I , and L_{II} are the magnetic-field coupling constant, the primary and the secondary inductances of the transformer. The ratio of the power being detected in L_i to the power sent from L_p to L_0 is the forward power transfer function $H_p^{I,II}(\omega)$ of the transformer and can be shown to be given by a frequency-independent expression

$$H_p^{I,II} = \frac{k_t^2 \frac{L_i}{L_{II}}}{\left[\frac{L_i}{L_{II}} + 1 - k_t^2 \right] \left[\frac{L_i}{L_{II}} + 1 \right]}. \quad (76)$$

The equivalent current noise for $S_I(\omega)$ seen by the transducer is therefore given by

$$S_I'(\omega) \equiv \frac{L_i S_I(\omega)}{L_0 H_p^{I,II}} = \frac{2E_A(\omega)}{L_0 H_p^{I,II}}. \quad (77)$$

Now, the circuit in Fig. 4(a) can be represented by an equivalent circuit with the transducer connected in series with L_0 and a current-to-voltage amplifier which has the equivalent current noise $S_I'(\omega)$, as shown in Fig. 4(b).

The quantity of interest is the equivalent (differential) acceleration noise at the transducer that would correspond to the amplifier noise of Eq. (77). The conversion from current noise to differential acceleration noise is made by use of the transfer function of the transducer, Eq. (53):

$$S_g^A(\omega) = \left[\frac{(\omega_0^2 - \omega^2)(L_0 + L_p)}{\Lambda I'} \right]^2 \frac{2E_A(\omega)}{L_0 H_p^{I,II}}. \quad (78)$$

For $\omega \ll \omega_0$, substitution of Eq. (73b) reduces this amplifier noise term to

$$S_g^A(\omega) = \frac{4}{m} \frac{\omega_0^2}{2\beta\eta} E_A(\omega), \quad (79)$$

where

$$\eta \equiv \frac{L_0}{L_0 + L_p} H_p^{I, \Pi} \quad (80)$$

is the fraction of electrical energy coupled to the amplifier. The product $\beta\eta$ represents the fraction of the total electromechanical energy coupled to the SQUID input, or the “SQUID energy coupling coefficient.”

There are three factors to optimize. The transfer function (75) is optimized when the transformer secondary is

$$(L_{II})_{\text{opt}} = \frac{L_i}{(1 - k_t^2)^{1/2}}, \quad (81)$$

yielding

$$(H_p^{I, \Pi})_{\text{opt}} = \frac{k_t^2}{[1 + (1 - k_t^2)^{1/2}]^2}. \quad (82)$$

From Eqs. (75) and (81) the transformer primary is chosen according to

$$(L_I)_{\text{opt}} = \frac{L_0}{(1 - k_t^2)^{1/2}}. \quad (83)$$

The impedance factor $L_0/(L_0 + L_p)$ in Eq. (80) is maximized by choosing $L_0 \gg L_p$. Finally, the frequency factor assumes a minimum:

$$\left[\frac{\omega_0^2}{2\beta} \right]_{\text{min}} = \omega_0^2, \quad (84)$$

when I' is chosen such that $\beta = \frac{1}{2}$: namely,

$$\frac{\Lambda^2 I'^2}{m(L_0 + L_p)} = \frac{1}{2} \omega_0^2. \quad (85)$$

This last optimization is applicable *only when the amplifier noise is dominating*.

C. Potential sensitivity

The fundamental noise of the gradiometer is the sum of its Brownian motion noise and SQUID amplifier noise. In terms of an equivalent gravity gradient noise Γ_n , the spectral density of the gradiometer noise is

$$S_{\Gamma}(\omega) = \frac{1}{l^2} [S_g^T(\omega) + S_g^A(\omega)], \quad (86)$$

where l is the length of the base line between the two proof masses. Substitution from Eqs. (71) and (79) gives the one-sided noise spectral density:

$$S_{\Gamma}(f) = \frac{4}{ml^2} \left[\frac{k_B T}{\tau(f)} + \frac{\omega_0^2}{2\beta\eta} E_A(f) \right], \quad (87)$$

where a factor 2π has been dropped from Eq. (71) by going from the angular frequency domain to the frequency domain. Here the numeral 4 will become 8 if m_1 is used instead of the reduced mass m .

In the usual case when $\tau_M \geq \tau_I$, the optimum value for I' satisfies an inequality:

$$0 < \frac{\Lambda^2 I'_{\text{opt}}{}^2}{m(L_0 + L_p)} < \frac{1}{2} \omega_0^2. \quad (88)$$

Toward the lower bound, the power coupled to the SQUID tends to zero. Toward the upper bound, the Brownian motion noise term increases because of the relatively short τ_I . If the amplifier noise dominates, the choice is made at the upper bound. If this bound is exceeded, the electromechanical spring has become so stiff that a given acceleration signal applied to the proof mass is producing less displacement, thus making it more difficult for the superconducting circuit to measure.

The SQUID input energy sensitivity $E_A(f)$ is usually a white noise plus a $1/f$ noise at very low frequencies. In addition, a dc drift can be caused by a temperature drift of the gradiometer.¹⁴ The drift changes the penetration depth and hence the inductances of the superconducting circuit.²⁴ Temperature related drifts can be suppressed by regulating the temperature or be balanced out with an improved circuit.²⁵ This and other errors are the subject that will be considered in Sec. V. The noise given in Eq. (87) represents the fundamental noise of the gradiometer which can be reached only when other instrument errors are suppressed sufficiently. However, having very low fundamental noise in the gradiometer itself is a prerequisite for achieving the desired high sensitivity.

V. ERROR MODEL OF THE INSTRUMENT

As we have seen in Sec. II, the gradiometer measures in general a differential gravity signal superposed with specific pseudoforces such as centrifugal acceleration and angular acceleration. In addition, the large dc gravity bias is modulated by the motion of the platform, resulting in error signals which compete with the ac signals under investigation. Thermal and electromagnetic fluctuations of the environment can also be coupled to the gradiometer. It is important to have a complete error model of the instrument because, for many applications, errors could dominate over the gravity gradient signals and therefore must be compensated for to recover the true signals. We start this section with a derivation of general expressions for the driving accelerations $g_d(t)$ and $g_c(t)$. We will then elaborate on specific error sources. The kinematic and dynamic error mechanisms discussed in this section are independent of the particular electrical circuit chosen for the superconducting gradiometer. Hence our results have general applicability beyond the specific instrument discussed in this paper.

A. Geometrical metrology errors

Let us consider the case in which the gradiometer is used to measure a time-varying in-line component gravity gradient at \mathbf{r} in the direction of a unit vector $\hat{\mathbf{n}}$ fixed in the laboratory frame:

$$\Gamma_{nn}(\mathbf{r}, t) = -(\hat{\mathbf{n}} \cdot \nabla)^2 \phi(\mathbf{r}, t). \quad (89)$$

Let \mathbf{r}_1 and \mathbf{r}_2 represent the *actual* position vectors for the centers of mass of the two proof masses m_1 and m_2 , and $\hat{\mathbf{n}}_1$ and $\hat{\mathbf{n}}_2$ be the unit vectors representing the *actual* sen-

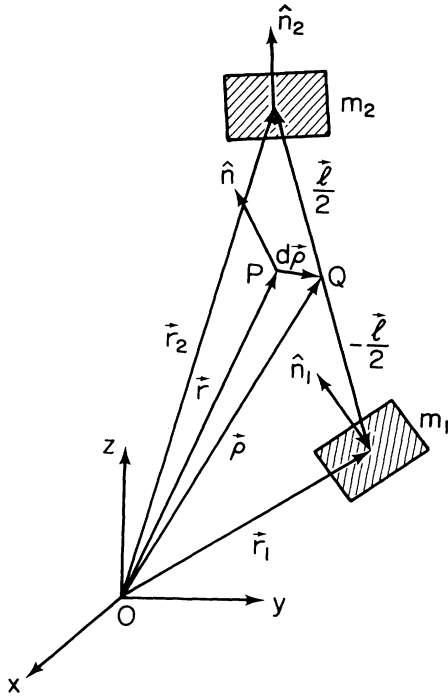


FIG. 5. Position, orientation, and sensitive axes alignment of the gradiometer.

sitive axes of the two component accelerometers, as indicated in Fig. 5. Let ρ and l represent the average proof mass position vector and the base line vector of the gradiometer, respectively, so that

$$\mathbf{r}_1 \equiv \rho - \frac{l}{2}, \quad (90a)$$

$$\mathbf{r}_2 \equiv \rho + \frac{l}{2}. \quad (90b)$$

Ideally, one wants $\rho = \mathbf{r}$. In general, one has a *gradiometer*

$$\begin{aligned} \mathbf{g}'(\mathbf{r}_1, t) = & -\nabla \left[1 - \left[\frac{l}{2} \cdot \nabla \right] + \frac{1}{2!} \left[\frac{l}{2} \cdot \nabla \right]^2 - \frac{1}{3!} \left[\frac{l}{2} \cdot \nabla \right]^3 + \cdots \right] \left\{ \phi(\rho, t) - \boldsymbol{\Omega}(t) \times \left[\boldsymbol{\Omega}(t) \times \left[\rho - \frac{l}{2} \right] \right] \right\} \\ & - \mathbf{a}(t) \times \left[\rho - \frac{l}{2} \right] - \mathbf{a}(t), \end{aligned} \quad (95a)$$

$$\begin{aligned} \mathbf{g}'(\mathbf{r}_2, t) = & -\nabla \left[1 + \left[\frac{l}{2} \cdot \nabla \right] + \frac{1}{2!} \left[\frac{l}{2} \cdot \nabla \right]^2 + \frac{1}{3!} \left[\frac{l}{2} \cdot \nabla \right]^3 + \cdots \right] \left\{ \phi(\rho, t) - \boldsymbol{\Omega}(t) \times \left[\boldsymbol{\Omega}(t) \times \left[\rho + \frac{l}{2} \right] \right] \right\} \\ & - \mathbf{a}(t) \times \left[\rho + \frac{l}{2} \right] - \mathbf{a}(t), \end{aligned} \quad (95b)$$

where we dropped the Coriolis terms assuming a rectilinear compliance of the proof mass suspension. In general, ρ and l are also time varying due to the translational and rotational motions of the platform with respect to an iner-

position error $\delta\rho$:

$$\rho \equiv \mathbf{r} + \delta\rho. \quad (91)$$

Likewise, in an ideal gradiometer, $\hat{\mathbf{n}}_1, \hat{\mathbf{n}}_2$ and $\hat{l} \equiv l/l$ are perfectly aligned to each other and are oriented along $\hat{\mathbf{n}}$. In a practical gradiometer, however, there are various alignment and orientation errors. The *axes alignment errors* consist of the misalignment between the sensitive axes of the two accelerometers,

$$\delta\hat{\mathbf{n}}_- \equiv \hat{\mathbf{n}}_2 - \hat{\mathbf{n}}_1, \quad (92)$$

and the misalignment between the average direction of the sensitive axes and the direction of the base line $\hat{l} \equiv l/l$:

$$\delta\hat{\mathbf{n}}_{+\hat{l}} \equiv \frac{1}{2}(\hat{\mathbf{n}}_2 + \hat{\mathbf{n}}_1) - \hat{l}. \quad (93)$$

These alignment errors will be shown to cause coupling to the gravity gradient output from the common linear acceleration component along the $\delta\hat{\mathbf{n}}_-$ direction and from the angular acceleration component along the $\delta\hat{\mathbf{n}}_{+\hat{l}} \times \hat{\mathbf{n}}$ direction. The *gradiometer orientation error* is due to the directions \hat{l} and $(\hat{\mathbf{n}}_2 + \hat{\mathbf{n}}_1)/2$ being misoriented from $\hat{\mathbf{n}}$ by $\delta\hat{l}$ and $\delta\hat{\mathbf{n}}_{+\hat{\mathbf{n}}}$, respectively,

$$\hat{l} \equiv \hat{\mathbf{n}} + \delta\hat{l}, \quad (94a)$$

$$\frac{1}{2}(\hat{\mathbf{n}}_2 + \hat{\mathbf{n}}_1) \equiv \hat{\mathbf{n}} + \delta\hat{\mathbf{n}}_{+\hat{\mathbf{n}}}, \quad (94b)$$

and will be shown to cause coupling from the differential acceleration component along the $\delta\hat{l} + \delta\hat{\mathbf{n}}_{+\hat{\mathbf{n}}}$ direction. Notice that only one of the two quantities $\delta\hat{l}$ and $\delta\hat{\mathbf{n}}_{+\hat{\mathbf{n}}}$ in conjunction with the misalignment $\delta\hat{\mathbf{n}}_{+\hat{l}}$ in Eq. (93) is sufficient to define the misorientation of the gradiometer. Introducing additional notations in Eqs. (94), however, has the advantage of simplifying expressions for misorientation errors by avoiding explicit reference to the misalignment parameters, defined within the gradiometer hardware.

In order to find the specific forces acting on m_1 and m_2 , Eqs. (90) are substituted into Eq. (4). After Taylor-series expansion in l , one finds

tial frame.

In Sec. III B, we defined as the acceleration signal the time-varying part over the constant background gravity of Earth. Since we are now interested in the mechanisms

which modulate the Earth's bias to produce error signals, we consider in this section the response of the gradiometer to the *total* accelerations:

$$\mathbf{g}'_k(t) \equiv \hat{\mathbf{n}}_k \cdot \mathbf{g}'(\mathbf{r}_k, t) = g_k(t) + \hat{\mathbf{n}} \cdot \mathbf{g}_E(\mathbf{r}). \quad (96)$$

We return at the end to the signal variables $g_k(t)$ to connect back to the analyses presented in earlier sections. With Earth's gravity vector $\mathbf{g}_E(\mathbf{r})$ as defined by Eq. (28), the last equality in Eq. (96) can be viewed as a rigorous redefinition of $g_k(t)$. Here a point-mass (or a spherical-mass) approximation of the proof masses has been used to avoid volume integration of $\mathbf{g}'(\mathbf{r}_k, t)$ over the finite dimensions of the proof masses.

The *total* common and differential accelerations for the *gradiometer*, defined in a similar fashion as $g_c(t)$ and $g_d(t)$ in Eq. (40), can now be shown to be

$$g'_c(t) = (\hat{\mathbf{n}} + \delta\hat{\mathbf{n}}_{+\hat{\mathbf{n}}}) \cdot \mathbf{g}'_{Cl}(\boldsymbol{\rho}, t) + \frac{1}{4} \delta\hat{\mathbf{n}}_- \cdot \mathbf{g}'_{Dl}(\boldsymbol{\rho}, t), \quad (97a)$$

$$g'_d(t) = \delta\hat{\mathbf{n}}_- \cdot \mathbf{g}'_{Cl}(\boldsymbol{\rho}, t) + (\hat{\mathbf{n}} + \delta\hat{\mathbf{n}}_{+\hat{\mathbf{n}}}) \cdot \mathbf{g}'_{Dl}(\boldsymbol{\rho}, t), \quad (97b)$$

where $\mathbf{g}'_{Cl}(\boldsymbol{\rho}, t)$ and $\mathbf{g}'_{Dl}(\boldsymbol{\rho}, t)$ are the *total true* common and differential accelerations acting at $\boldsymbol{\rho} \pm \mathbf{l}/2$:

$$\mathbf{g}'_c(t) = (\hat{\mathbf{n}} + \delta\hat{\mathbf{n}}_{+\hat{\mathbf{n}}}) \cdot \mathbf{g}'(\mathbf{r} + \delta\boldsymbol{\rho}, t) + \frac{1}{4} \delta\hat{\mathbf{n}}_- \cdot \vec{\Gamma}'(\mathbf{r} + \delta\boldsymbol{\rho}, t) \cdot (\hat{\mathbf{n}} + \delta\hat{\mathbf{l}}) - \frac{1}{4} \delta\hat{\mathbf{n}}_- \cdot \boldsymbol{\alpha} \times (\hat{\mathbf{n}} + \delta\hat{\mathbf{l}}) + \delta g_{c,l}, \quad (100a)$$

$$\mathbf{g}'_d(t) = \delta\hat{\mathbf{n}}_- \cdot \mathbf{g}'(\mathbf{r} + \delta\boldsymbol{\rho}, t) + \mathbf{l} \cdot (\hat{\mathbf{n}} + \delta\hat{\mathbf{n}}_{+\hat{\mathbf{n}}}) \cdot \vec{\Gamma}'(\mathbf{r} + \delta\boldsymbol{\rho}, t) \cdot (\hat{\mathbf{n}} + \delta\hat{\mathbf{l}}) - \mathbf{l} \delta\hat{\mathbf{n}}_{+\hat{\mathbf{n}}} \cdot \boldsymbol{\alpha} \times (\hat{\mathbf{n}} + \delta\hat{\mathbf{l}}) + \delta g_{d,l}. \quad (100b)$$

Here \mathbf{g}' and $\vec{\Gamma}'$ are the specific force vector and the specific force gradient tensor defined in Eqs. (4) and (8); $\delta g_{c,l}$ and $\delta g_{d,l}$ are the finite-size terms given in Eqs. (A1). Equation (100b) shows that the "sensitive axis of the gradiometer" can be defined by the average of $(\hat{\mathbf{n}}_1 + \hat{\mathbf{n}}_2)/2$ and $\hat{\mathbf{l}}$.

B. General description of errors

The accelerations in Eqs. (100) contain two types of error sources. The first type is intrinsic error sources due to angular motions as given in Eqs. (4) and (8), while the second type is in geometrical metrology. Further error sources arise from nonideal behavior of the mechanical and electrical springs, scale factor mismatch, incorrect calibration, and residual coupling of the gradiometer to temperature, and electromagnetic fluctuations of the environment, etc. Equation (45) can therefore be generalized as

$$i_d(\omega) = H_{g_i^c}^c(\omega) g_c(\omega) + H_{g_i^d}^d(\omega) g_d(\omega) + H_{G_i^c}^{cc}(\omega) G_{cc}(\omega) + H_{G_i^d}^{dd}(\omega) G_{dd}(\omega) + H_{G_i^c}^{cd}(\omega) G_{cd}(\omega) + H_{T_i^c}^c(\omega) T_c(\omega) + H_{T_i^d}^d(\omega) T_d(\omega) + \dots, \quad (101)$$

where $G_{cc}(\omega)$, $G_{dd}(\omega)$, and $G_{cd}(\omega)$ are the Fourier transforms of

$$G_{cc}(t) \equiv [g_c(t)]^2, \quad (102a)$$

$$G_{dd}(t) \equiv [g_d(t)]^2, \quad (102b)$$

$$G_{cd}(t) \equiv g_c(t) g_d(t), \quad (102c)$$

and $T_c(\omega)$ and $T_d(\omega)$ are the Fourier transforms of the common and differential temperature fluctuations, $T_c(t)$ and $T_d(t)$, over the two transducers, defined in Eqs. (A26). The coefficients in front of these functions represent the transfer functions for the signal variables with which they are multiplied. The centrifugal acceleration and the linear and angular accelerations, which are coupled to the gradiometer due to its metrology errors,

$$\mathbf{g}'_{Cl}(\boldsymbol{\rho}, t) = -\nabla \left[1 + \frac{1}{2!} \left[\frac{\mathbf{l}}{2} \cdot \nabla \right]^2 + \dots \right] \phi(\boldsymbol{\rho}) - \mathbf{a}(\boldsymbol{\rho}), \quad (98a)$$

$$\mathbf{g}'_{Dl}(\boldsymbol{\rho}, t) = -\nabla \left[(\mathbf{l} \cdot \nabla) + \frac{2}{3!} \left[\frac{\mathbf{l}}{2} \cdot \nabla \right]^3 + \dots \right] \phi(\boldsymbol{\rho}) - \boldsymbol{\Omega} \times (\boldsymbol{\Omega} \times \mathbf{l}) - \boldsymbol{\alpha} \times \mathbf{l}. \quad (98b)$$

Here $\mathbf{a}(\boldsymbol{\rho})$ is the total linear acceleration experienced at $\boldsymbol{\rho}$:

$$\mathbf{a}(\boldsymbol{\rho}) \equiv \boldsymbol{\Omega} \times (\boldsymbol{\Omega} \times \boldsymbol{\rho}) + \boldsymbol{\alpha} \times \boldsymbol{\rho} + \mathbf{a}, \quad (99)$$

and the time dependencies have been omitted on the right-hand side of Eqs. (98) for notational simplicity.

Equations (97)–(99) are in the platform frame representation. It is straightforward to convert these equations into the laboratory frame representation by substituting Eqs. (91), (93), and (94). The relative uncertainties between the two frames, $\delta\boldsymbol{\rho}$, $\delta\hat{\mathbf{n}}_{+\hat{\mathbf{n}}}$, and $\delta\hat{\mathbf{l}}$, then constitute new error sources. Thus, it can be shown that Eqs. (97) become

appear in Eq. (101) through errors in $g_c(\omega)$ and $g_d(\omega)$ that they cause.

Notice that Eq. (101) contains the original signal variables, $g_c(\omega)$ and $g_d(\omega)$, which are identical to $g'_c(\omega)$ and $g'_d(\omega)$ due to the relationships

$$g_c(t) = g'_c(t) - \hat{\mathbf{n}} \cdot \mathbf{g}_E(\mathbf{r}), \quad (103a)$$

$$g_d(t) = g'_d(t), \quad (103b)$$

which follow from Eq. (96). Equations (103) imply that the errors in the unprimed variables are given by the errors in the primed variables:

$$\delta g_c(t) = \delta g'_c(t), \quad (104a)$$

$$\delta g_d(t) = \delta g'_d(t). \quad (104b)$$

It is also clear that the Fourier components of the errors are also identical between the two sets of variables. Equations (100) and (103) can be combined to obtain the unperturbed acceleration signals:

$$g_{c0}(\omega) = g'_{c0}(\omega) = \hat{\mathbf{n}} \cdot [\mathbf{g}(\mathbf{r}, \omega) - \mathbf{a}(\mathbf{r}, \omega)], \quad (105a)$$

$$g_{d0}(\omega) = g'_{d0}(\omega) = l \hat{\mathbf{n}} \cdot [\vec{\Gamma}(\mathbf{r}, \omega) - \vec{\mathbf{C}}(\omega)] \cdot \hat{\mathbf{n}}, \quad (105b)$$

where $\mathbf{g}(\mathbf{r}, \omega)$, $\mathbf{a}(\mathbf{r}, \omega)$, $\vec{\Gamma}(\mathbf{r}, \omega)$, and $\vec{\mathbf{C}}(\omega)$ are the Fourier transforms of

$$\mathbf{g}(\mathbf{r}, t) \equiv -\nabla\phi(\mathbf{r}, t) = -\nabla\phi_p(\mathbf{r}, t) - \nabla\phi_E(\mathbf{r}), \quad (106a)$$

$$\mathbf{a}(\mathbf{r}, t) = \mathbf{a}_p(\mathbf{r}, t) + \Omega_E \times [\Omega_E \times (\mathbf{R}_E + \mathbf{r})], \quad (106b)$$

$$\vec{\Gamma}(\mathbf{r}, t) \equiv -\nabla\nabla\phi(\mathbf{r}, t) = -\nabla\nabla\phi_p(\mathbf{r}, t) - \nabla\nabla\phi_E(\mathbf{r}), \quad (106c)$$

$$\vec{\mathbf{C}}(t) \equiv \Omega(t)\Omega(t) - \Omega^2(t)\vec{\mathbf{I}}$$

$$= \begin{bmatrix} -\Omega_y^2 - \Omega_z^2 & \Omega_x\Omega_y & \Omega_x\Omega_z \\ \Omega_x\Omega_y & -\Omega_z^2 - \Omega_x^2 & \Omega_y\Omega_z \\ \Omega_x\Omega_z & \Omega_y\Omega_z & -\Omega_x^2 - \Omega_y^2 \end{bmatrix}. \quad (106d)$$

Here $\phi_E(\mathbf{r})$, Ω_E , and \mathbf{R}_E are Earth's variables introduced in Eq. (28); $\phi_p(\mathbf{r}, t)$ and $\mathbf{a}_p(\mathbf{r}, t)$ are the gravitational potential and the linear acceleration measured relative to Earth; and $\vec{\mathbf{C}}(t)$ is the "centrifugal acceleration tensor." The dyadic notation is used in Eqs. (106) to represent rank-2 tensors. The first term in Eq. (105b) is l times the gravity gradient signal $\Gamma_{nn}(\mathbf{r}, \omega)$ to be measured.

It is useful to divide Eq. (101) by $lH_{gi}^d(\omega)$ to obtain an equation of the form

$$[\Gamma_{nn}(\mathbf{r}, \omega)]_{\text{measured}} \equiv \frac{1}{l} \frac{i_d(\omega)}{H_{gi}^d(\omega)} = [\Gamma_{nn}(\mathbf{r}, \omega)]_{\text{true}} + \frac{1}{l} \sum_i \delta g_{d,i}(\omega), \quad (107)$$

where $\delta g_{d,i}(\omega)$ is the *equivalent* error in the differential acceleration $g_d(\omega)$ due to the i th-type error source. Derivation and discussion of $\delta g_{d,i}$ for various error sources are given in the Appendix. Equation (107) can be converted into another convenient form:

$$\delta\Gamma_{nn}(\mathbf{r}, \omega) = \sum_{l,m} \epsilon_{nlm}^{\Gamma}(\omega) \Gamma_{lm}(\mathbf{r}, \omega) + \sum_{l,m} \epsilon_{nlm}^C(\omega) C_{lm}(\omega) + \sum_l \epsilon_{nl}^a(\omega) a_l(\mathbf{r}, \omega) + \sum_l \epsilon_{nl}^{\Omega}(\omega) \Omega_{p,l}(\omega) + \epsilon_n^T(\omega) T_c(\omega) + \dots, \quad (108)$$

in which dominant error sources have been shown explicitly. Here the laboratory has been assumed to be stationary with respect to Earth and $\Omega_p(\omega)$ is the angular velocity of the platform in the laboratory frame. The first two error coefficients can be identified from Eqs. (A6b) and (A19):

$$\epsilon_{nlm}^{\Gamma}(\omega) = \delta_{ln} \delta_{mn} \delta\sigma_{\Gamma}(\omega) + (1 - \delta_{ln}) \delta_{mn} (\delta\hat{\mathbf{n}}_{+\hat{\mathbf{n}}} + \delta\hat{\mathbf{l}})_l, \quad (109a)$$

$$\epsilon_{nlm}^C(\omega) = -\delta_{ln} \delta_{mn} \delta\sigma_C(\omega) - (1 - \delta_{ln}) \delta_{mn} (\delta\hat{\mathbf{n}}_{+\hat{\mathbf{n}}} + \delta\hat{\mathbf{l}})_l, \quad (109b)$$

where $\delta\sigma_{\Gamma}(\omega)$ and $\delta\sigma_C(\omega)$ are the (dimensionless) calibration error coefficients for $\vec{\Gamma}(\mathbf{r}, \omega)$ and $\vec{\mathbf{C}}(\omega)$, respectively. It is assumed that the zeroth-order part of $\vec{\mathbf{C}}(\omega)$ has been measured independently and removed from the gradiometer output. Otherwise, $\delta\sigma_C(\omega)$ must be replaced by unity. The common acceleration error coefficient is read off Eq. (A21):

$$\epsilon_{nl}^a(\omega) = -\delta_{ln} \frac{1}{l} \delta\sigma_S(\omega) - (1 - \delta_{ln}) \frac{1}{l} (\delta\hat{\mathbf{n}}_-)_l, \quad (109c)$$

where $\delta\sigma_S(\omega)$ is the (dimensionless) scale factor mismatch between two constituent accelerometers. The coefficient for the first-order angular velocity induced error is obtained from Eqs. (A10) and (A12):

$$\begin{aligned} \epsilon_{nl}^{\Omega}(\omega) &= (1 - \delta_{ln}) 2\Omega_{E,l} \\ &\quad - \frac{1}{j\omega l} \sum_{k,m} (1 - \delta_{kn}) \epsilon_{klm} (\delta\hat{\mathbf{n}}_-)_k g_{E,m}(\mathbf{r}) \\ &\quad + j\omega \sum_k (1 - \delta_{kn}) \epsilon_{kln} (\delta\hat{\mathbf{n}}_{+\hat{\mathbf{l}}})_k, \end{aligned} \quad (109d)$$

where $\delta\Omega_p = \Omega_p$ has been assumed and ϵ_{klm} is the totally antisymmetric tensor of rank 3.

Unlike in some conventional gravity gradiometers, matching of proof masses and spring constants are *not* necessary in the superconducting device because the balance is achieved by tuning persistent currents. However, the alignment of the sensitive axes of the proof masses is still important.

The temperature-error coefficient can be determined from the results of Sec. 8 of the Appendix. Depending on the relative magnitude of the two competing thermal effects, the error coefficient can be written as

$$\epsilon_n^T(\omega) = \frac{1}{l} h_{T_c}(\omega), \quad (109e)$$

where $h_{T_c}(\omega)$ is given by Eq. (A42a), or by

$$\epsilon_n^T(\omega) = \frac{1}{l} \delta\sigma_S(\omega) g_E \cos\theta_n \frac{1}{E(T)} \frac{dE}{dT}, \quad (109e')$$

where $E(T)$ is the Young's modulus of the spring material at temperature T .

In paper II we discuss the observed values or limits of these major error coefficients. Once these error coefficients have been determined experimentally, the relevant

dynamic variables can be measured simultaneously along with the gravity gradient by independent instrumentation and the respective errors can be compensated for by using the error model derived in this section and the Appendix. In a three-axis gradiometer, it is possible to suppress several error sources by using the geometrical properties of the device.¹⁸

VI. SUMMARY AND CONCLUSION

A gravity gradiometer is a fundamental instrument which can separate gravity from frame accelerations. A sensitive tensor gravity gradiometer needs to be developed to carry out precision tests on gravity as well as for applications in gravity survey and inertial navigation. Since a large common mode background has to be removed in gradiometry by differencing signals at two or more proof masses, extreme stability is required for the sensitive axis orientation and for the scale factors of the component accelerometers. We have shown how these challenges can be met at low temperatures by utilizing the stability of persistent currents, the enhanced mechanical stability of materials, and the sensitivity of SQUID amplifiers. An accompanying penalty is of course the inconvenience of having to keep the instrument in liquid helium. The liquid-helium environment, however, can be used further to isolate the gradiometer from the fluctuations in the ambient temperature and electromagnetic fields.

In this paper we have analyzed a superconducting current-differencing gravity gradiometer. Complete dynamical equations have been derived from first principles. Transfer functions, common mode balance conditions, and procedures, as well as a rather extensive error model have been developed from these equations. The complicated differential instrument has been reduced to an equivalent accelerometer which simplifies the noise analysis and the electronic control of the device. In paper II we report the performance of the superconducting gradiometer in the laboratory, which verifies details of the theory developed here. Although our analysis has been confined to a specific instrument reported in paper II, the theoretical methods presented in this paper will be a useful guide in analyzing other superconducting inertial instruments that may be developed in the future.

ACKNOWLEDGMENTS

We would like to thank Professor Daniel DeBra and Professor Alex Dragt for valuable suggestions. We also thank Dr. M. V. Moody for fruitful collaboration in the experiment which checks the theory developed here. This work was supported by NASA under Contract No. NAS 8-33822.

APPENDIX: DERIVATION OF VARIOUS ERROR COEFFICIENTS

1. Finite-size effects

There are two error sources related to the finite dimensions of a practical gradiometer: (1) the *finite volume* of the proof masses and (2) the *finite base line* of the instru-

ment. The first effect can be minimized by choosing a nearly spherical geometry for the proof masses, whereas the second effect is reduced when the base line length $l = |l|$ is shortened. The finite-base line effect has been taken into account in Eqs. (95) by the Taylor expansion in l . The finite-volume effect has been ignored in the previous analysis because of its high-order nature. The departure from a spherical geometry gives a nonvanishing quadrupole moment to each proof mass or a small octupole moment to the gradiometer. Since this will couple at best to the fourth-order derivatives of $\phi(\rho, t)$, which is generally small except when the source is extremely close to the gradiometer, this error can be ignored in most situations. Clearly, the finite-volume error is always smaller than the finite-base line error.

The dominant gravity error terms arising from the finite base line are obtained from Eqs. (97) and (98):

$$\delta g_{c,l}(t) = -\frac{l^2}{8} (\hat{l} \cdot \nabla)^3 \phi(\rho, t), \quad (\text{A1a})$$

$$\delta g_{d,l}(t) = -\frac{l^3}{24} (\hat{l} \cdot \nabla)^4 \phi(\rho, t). \quad (\text{A1b})$$

When $\phi(\rho, t)$ varies with a characteristic length R , these errors become $O(l^2/R^2)$ of the signal. Therefore, the finite base line error can also be ignored when $l/R \ll 1$.

2. Misposition of the gradiometer

The acceleration errors due to the *misposition* of the gradiometer are obtained from Eqs. (4) and (100):

$$\delta g_{c,\rho}(t) = -\hat{n} \cdot [\nabla \nabla \phi(\mathbf{r}) + \Omega \Omega - \Omega^2 \hat{\mathbf{I}}] \cdot \delta \rho - \hat{n} \cdot \alpha \times \delta \rho, \quad (\text{A2a})$$

$$\delta g_{d,\rho}(t) = -l (\hat{n} \cdot \nabla) [\hat{n} \cdot \nabla \nabla \phi(\mathbf{r}) \cdot \delta \rho], \quad (\text{A2b})$$

to the leading order in $\delta \rho$. These errors are usually negligible because of the higher-order gradients involved. The displacement $\delta \rho(t)$, produced by the linear acceleration $\mathbf{a}(\mathbf{r}, t)$, modulates the large dc gravity of Earth and produces errors that compete with ac signals:

$$\delta g_{c,\rho}(t) = O \left[\frac{\delta \rho(t)}{R_E} g_E \right], \quad (\text{A3a})$$

$$\delta g_{d,\rho}(t) = O \left[\frac{\delta \rho(t)}{R_E} l \Gamma_E \right], \quad (\text{A3b})$$

where $g_E \equiv 9.8 \text{ m sec}^{-2}$, $\Gamma_E \equiv 3.1 \times 10^3 \text{ E}$, and $R_E \equiv 6.4 \times 10^6 \text{ m}$ are the vertical gravitational acceleration, the vertical gravity gradient, and the radius of Earth. It is clear that these errors can be ignored in general because $\delta \rho(t)/R_E \ll 1$.

3. Misalignment and misorientation of the gradiometer

The acceleration errors caused by the *misalignments*, $\delta \hat{n}_-$ and $\delta \hat{n}_{+\hat{\gamma}}$, and the *misorientations*, $\delta \hat{n}_{+\hat{n}}$, and $\delta \hat{l}$, are obtained from Eqs. (100):

$$\begin{aligned} \delta g_{c,\hat{n}+\hat{l}}(t) = & \delta \hat{n}_{+\hat{n}} \cdot \mathbf{g}'(\mathbf{r},t) + \frac{l}{4} \delta \hat{n}_{-} \cdot \vec{\Gamma}'(\mathbf{r},t) \cdot \hat{n} \cdot \vec{\Gamma}'(\mathbf{r},t) \cdot \hat{n} \\ & - \frac{l}{4} \delta \hat{n}_{-} \cdot \boldsymbol{\alpha} \times \hat{n}, \end{aligned} \quad (\text{A4a})$$

$$\begin{aligned} \delta g_{d,\hat{n}+\hat{l}}(t) = & \delta \hat{n}_{-} \cdot \mathbf{g}'(\mathbf{r},t) + l(\delta \hat{n}_{+\hat{n}} + \delta \hat{l}) \cdot \vec{\Gamma}'(\mathbf{r},t) \cdot \hat{n} \\ & - l \delta \hat{n}_{+\hat{l}} \cdot \boldsymbol{\alpha} \times \hat{n}, \end{aligned} \quad (\text{A4b})$$

to the leading order in $\delta \hat{n}_{-}, \delta \hat{n}_{+\hat{l}}, \delta \hat{n}_{+\hat{n}}$. It follows from the definitions (92)–(94) that, in the limits $|\delta \hat{n}_{-}|, |\delta \hat{n}_{+\hat{l}}|, |\delta \hat{n}_{+\hat{n}}|, |\delta \hat{l}| \ll 1$,

$$\delta \hat{n}_{-}, \delta \hat{n}_{+\hat{l}}, \delta \hat{n}_{+\hat{n}}, \delta \hat{l} \perp \hat{n}. \quad (\text{A5})$$

Hence these errors cause the cross components of the common acceleration and the acceleration gradient to couple to the gradiometer. Written out explicitly, Eqs. (A4) become

$$\begin{aligned} \delta g_{c,\hat{n}+\hat{l}}(t) = & -\delta \hat{n}_{+\hat{n}} \cdot [\nabla \phi(\boldsymbol{\rho}) + \mathbf{a}(\boldsymbol{\rho})] \\ & - \frac{l}{4} \delta \hat{n}_{-} \cdot [\nabla \nabla \phi(\boldsymbol{\rho}) + \boldsymbol{\Omega} \boldsymbol{\Omega}] \cdot \hat{n} \\ & + \frac{l}{4} \delta \hat{n}_{-} \times \hat{n} \cdot \boldsymbol{\alpha}, \end{aligned} \quad (\text{A6a})$$

$$\begin{aligned} \delta g_{d,\hat{n}+\hat{l}}(t) = & -\delta \hat{n}_{-} \cdot [\nabla \phi(\boldsymbol{\rho}) + \mathbf{a}(\boldsymbol{\rho})] \\ & - l(\delta \hat{n}_{+\hat{n}} + \delta \hat{l}) \cdot [\nabla \nabla \phi(\boldsymbol{\rho}) + \boldsymbol{\Omega} \boldsymbol{\Omega}] \cdot \hat{n} \\ & + l \delta \hat{n}_{+\hat{l}} \times \hat{n} \cdot \boldsymbol{\alpha}. \end{aligned} \quad (\text{A6b})$$

In Eq. (A6b) the misalignments *within* the gradiometer are expressed in terms of the misalignment $\delta \hat{n}_{-}$ of the accelerometer axes with respect to each other and the misalignment $\delta \hat{n}_{+\hat{l}}$ between the average accelerometer axis $(\hat{n}_1 + \hat{n}_2)/2$ and the base line direction \hat{l} . These errors cause coupling to cross components of linear and angular accelerations which can be large compared with acceleration gradient signals of interest. The combined error $\delta \hat{n}_{+\hat{n}} + \delta \hat{l}$ appearing in the second term of Eq. (A6b) represents the misorientation of the gradiometer sensitive axis relative to the *theoretical* direction \hat{n} fixed to the laboratory frame, which is used for interpreting the data. This misorientation produces coupling to cross gradients.

The coupling to the gradiometer from the dynamic variables of the platform, $\mathbf{a}(\boldsymbol{\rho},t)$, $\boldsymbol{\Omega}(t)$, and $\boldsymbol{\alpha}(t)$, are revealed in Eqs. (A6). Since \hat{l} and $\delta \hat{n}_{+}$ are time varying in general due to $\boldsymbol{\Omega}(t)$, the large dc gravity of Earth, $\phi_E(\boldsymbol{\rho})$, will be modulated to produce errors at the frequency of interest. This important error mechanism will be studied in detail in the next section.

4. Angular motions of the platform

The *centrifugal acceleration* appears without attenuation in Eq. (105b) in direct competition with the gravity

gradient signal. This problem is *fundamental* in any second-order gradiometer, in-line or cross component, as is evidenced by Eq. (9), and therefore does not depend on the particular design of the instrument. This makes the attitude control or detection as the most formidable task in precision gravity gradiometry. One can easily compute the required attitude rate ($\boldsymbol{\Omega}$) accuracy from Eq. (105b) for a given sensitivity of $\vec{\Gamma}$.

When the instrument is in a laboratory rotating at an angular velocity $\boldsymbol{\Omega}_0(t)$ with respect to an inertial frame, it is convenient to define

$$\boldsymbol{\Omega}(t) \equiv \boldsymbol{\Omega}_0(t) + \boldsymbol{\Omega}_P(t). \quad (\text{A7})$$

If uncertainties in $\boldsymbol{\Omega}_0(t)$ and $\boldsymbol{\Omega}_P(t)$ are $\delta \boldsymbol{\Omega}_0(t)$ and $\delta \boldsymbol{\Omega}_P(t)$, respectively, then the error in the differential acceleration due to centrifugal acceleration is obtained from Eqs. (105b), (106d), and (A7) as

$$\begin{aligned} \delta g_{d,\vec{c}}(t) = & -2l \{ [\hat{n} \cdot (\boldsymbol{\Omega}_0 + \boldsymbol{\Omega}_P)] [\hat{n} \cdot (\delta \boldsymbol{\Omega}_0 + \delta \boldsymbol{\Omega}_P)] \\ & - (\boldsymbol{\Omega}_0 + \boldsymbol{\Omega}_P) \cdot (\delta \boldsymbol{\Omega}_0 + \delta \boldsymbol{\Omega}_P) \}. \end{aligned} \quad (\text{A8})$$

If the gradiometer platform is moving with a velocity $\mathbf{v}(t)$ with respect to Earth and the gradiometer is in a local geographic orientation, then $\boldsymbol{\Omega}_0(t)$ is given by

$$\boldsymbol{\Omega}_0(t) = \boldsymbol{\Omega}_E + R_E^{-2} \mathbf{R}_E \times \mathbf{v}(t), \quad (\text{A9})$$

where $\boldsymbol{\Omega}_E$ and \mathbf{R}_E are the angular velocity and radius vectors of Earth, introduced in Eq. (28). In the case when the platform is stationary with respect to Earth; i.e., $\mathbf{v}(t) = 0$, Eq. (A8) reduces, after Fourier transformation, to

$$\delta g_{d,\vec{c}}(\omega) = -2l \{ (\hat{n} \cdot \boldsymbol{\Omega}_E) [\hat{n} \cdot \delta \boldsymbol{\Omega}_P(\omega)] - \boldsymbol{\Omega}_E \cdot \delta \boldsymbol{\Omega}_P(\omega) \}, \quad (\text{A10})$$

where we have assumed the condition $\boldsymbol{\Omega}_P \ll \boldsymbol{\Omega}_E = 7.27 \times 10^{-5} \text{ rad sec}^{-1}$, which is not difficult to satisfy for a stationary platform.

In a terrestrial laboratory the *modulation of Earth's gravity bias* by the tilt of the sensitive axes is another important error mechanism, as was pointed out in Sec. 3 of this appendix. Since the common-mode errors in Eq. (A6a) produce second-order errors in the differential signal when multiplied by the common-mode balance error H_{gi}^c according to Eq. (51), these errors will, in general, be dominated by the errors in Eq. (A6b), which is multiplied by H_{gi}^d .

When the platform moves at an angular velocity $\boldsymbol{\Omega}_P(t)$ with respect to the terrestrial laboratory, the misalignment and misorientation vectors are modulated according to

$$\frac{d}{dt} \mathbf{A} = \boldsymbol{\Omega}_P(t) \times \mathbf{A}, \quad (\text{A11a})$$

$$\frac{d}{dt} \mathbf{B} = \boldsymbol{\Omega}_P(t) \times \hat{n}, \quad (\text{A11b})$$

where \mathbf{A} stands for $\delta \hat{n}_{-}$ and $\delta \hat{n}_{+\hat{l}}$ and \mathbf{B} for $\delta \hat{n}_{+\hat{n}}$ and $\delta \hat{l}$. Equation (A6b) becomes, upon Fourier transformation,

$$\delta g_{d,\hat{n}+\hat{l}}(\omega) = -\delta \hat{n}_{-} \cdot \frac{\boldsymbol{\Omega}_P(\omega)}{j\omega} \times \mathbf{g}_E(\mathbf{r}) - 2l \hat{n} \cdot \frac{\boldsymbol{\Omega}_P(\omega)}{j\omega} \times [\vec{\Gamma}'_E(\mathbf{r}) \cdot \hat{n}] + l \delta \hat{n}_{+\hat{l}} \times \hat{n} \cdot [j\omega \boldsymbol{\Omega}_P(\omega)], \quad (\text{A12})$$

where $\mathbf{g}_E \equiv -\nabla\phi_E$, $\vec{\Gamma}_E \equiv -\nabla\nabla\phi_E$, and $\boldsymbol{\alpha}(\omega) \equiv j\omega\boldsymbol{\Omega}_P(\omega)$ were substituted. The term arising from the angular modulation of $\delta\hat{\mathbf{n}}_{+\hat{l}}$ produces a second-order effect in $\boldsymbol{\Omega}_P(\omega)$ and therefore has been dropped. In the case when

$$|\delta\hat{\mathbf{n}}_-| > \frac{2l\Gamma_E}{g_E} \simeq \frac{4l}{R_E}, \quad (\text{A13})$$

the second term in Eq. (A12) can be ignored. The third term becomes negligible compared to the first term at sufficiently low signal frequencies:

$$\omega < \left(\frac{g_E}{l} \right)^{1/2} \left| \frac{\delta\hat{\mathbf{n}}_-}{\delta\hat{\mathbf{n}}_{+\hat{l}}} \right|^{1/2}. \quad (\text{A14a})$$

Comparing Eq. (A12) with Eq. (A10), one finds that the time-varying tilt noise is the dominant source of angular motion induced errors in the frequency range

$$\omega \leq \frac{g_E}{l\Omega_E} |\delta\hat{\mathbf{n}}_-|, \quad (\text{A14b})$$

even when $\delta\boldsymbol{\Omega}_P = \boldsymbol{\Omega}_P$, the worst case for the centrifugal acceleration error. In paper II we will see that the angular motion noise given by Eq. (12) is indeed the dominant error mechanism for our prototype superconducting gravity gradiometer.

The foregoing discussion clearly reveals the advantage of operating a sensitive gradiometer in space where the gradiometer platform is freely falling. If an Earth-pointing reference frame is chosen so that $\boldsymbol{\Omega}_0(t)$ coincides with the orbital angular velocity of the satellite, then Eqs. (A8) and (A6b) reduce, respectively, to

$$[\delta g_{d,\vec{C}}(\omega)]_{\text{space}} = -2l \{ (\hat{\mathbf{n}} \cdot \boldsymbol{\Omega}_0) [\hat{\mathbf{n}} \cdot \delta\boldsymbol{\Omega}_P(\omega)] - \boldsymbol{\Omega}_0 \cdot \delta\boldsymbol{\Omega}_P(\omega) \}, \quad (\text{A15})$$

$$[\delta g_{d,\hat{\mathbf{n}}_{+\hat{l}}}(\omega)]_{\text{space}} = -2l\hat{\mathbf{n}}_{+\hat{l}} \cdot \frac{\boldsymbol{\Omega}_P(\omega)}{j\omega} \times [\vec{\Gamma}_E(\mathbf{r}) - \boldsymbol{\Omega}_0\boldsymbol{\Omega}_0] \cdot \hat{\mathbf{n}}_{+\hat{l}} + l\delta\hat{\mathbf{n}}_{+\hat{l}} \times \hat{\mathbf{n}}_{+\hat{l}} \cdot [j\omega\boldsymbol{\Omega}_P(\omega)], \quad (\text{A16})$$

where $\vec{\Gamma}_E(\mathbf{r})$ is the gravity gradient tensor of (spherical) Earth. Comparison of Eqs. (A15) and (A16) leads to a conclusion that the centrifugal acceleration error could be dominant in most practical cases.

One can see from Eq. (A8) that $\delta g_{d,\vec{C}}(t)$ has a minimum when the gradiometer is in an inertial orientation; i.e., $\boldsymbol{\Omega}_0 = 0$. The worst situation for the centrifugal acceleration error is the case when the gradiometer is rotated at a frequency high compared to the signal frequency for heterodyne detection of the gravity signal. In this case, $\boldsymbol{\Omega}_0$ is the spin angular velocity which is large compared to $\boldsymbol{\Omega}_E$. One advantage of the superconducting gravity gradiometer is that the heterodyne detection is *not necessary*, unlike in some conventional devices, because of its low drift and excellent low-frequency noise characteristics. The superconducting gradiometer therefore permits complete freedom in orientation: inertial, earth pointing, or spin stabilized.²⁶ Hence, an optimum orientation, which minimizes the overall error budget, is available to the su-

perconducting instrument although the angular motion induced errors are fundamental.

In Eqs. (A10) and (A15) we considered only the first-order errors in $\delta\boldsymbol{\Omega}_P(\omega)$. This is justified when $\delta\boldsymbol{\Omega}_P(\omega)$ is bandwidth limited. The Fourier transform of $[\delta\boldsymbol{\Omega}_P(t)]^2$ down converts the centrifugal acceleration noise from high frequencies to the vicinity of dc, the signal bandwidth. A low-pass filter for angular vibrations of the platform is therefore needed to suppress this error.

5. Scale factor errors

There are two types of *scale factor errors* in a gradiometer: (1) a *relative* error, which comes from the mismatch of the scale factors of the component accelerometers and (2) an *absolute* error, which is the error in the calibration of the gradiometer transfer function. Since the scale factors are determined by persistent currents in the superconducting gradiometer, extreme stability is expected in the scale factor match and calibration. The passive, iterative, common mode balance procedure described in Sec. III D allows in principle an arbitrarily precise match of scale factors in one direction independent of signal frequency. In practice, however, $H_{gi}^c(\omega)$ is not precisely zero in Eq. (101), thus producing a common mode rejection error, and $H_{gi}^d(\omega)$ also contains a calibration error $\delta H_{gi}^d(\omega)$.

Let us define the (dimensionless) coefficients for scale factor mismatch and gradiometer calibration error by

$$\delta\sigma_S(\omega) \equiv \frac{H_{gi}^c(\omega)}{H_{gi}^d(\omega)}, \quad (\text{A17a})$$

$$\delta\sigma_T(\omega) \equiv \frac{\delta H_{gi}^d(\omega)}{H_{gi}^d(\omega)} - \frac{\delta l}{l}, \quad (\text{A17b})$$

and for the centrifugal acceleration calibration error by $\delta\sigma_C(\omega)$, which is usually different from $\delta\sigma_T(\omega)$ because independent instruments, such as gyroscopes, are used to measure and compensate the effect. The error arising from the use of an inaccurate value of l in the recovery of $\Gamma_{nn}(\mathbf{r}, t)$ from $g_{d0}(t)$ in Eq. (105b) is represented by the second term in Eq. (A17b). With the aid of Eqs. (105), the *equivalent* differential acceleration errors due to *scale factor mismatch* and *calibration errors* can be written as

$$\delta g_{d,S}(\omega) = \delta\sigma_S(\omega) \hat{\mathbf{n}} \cdot [\mathbf{g}(\mathbf{r}, \omega) - \mathbf{a}(\mathbf{r}, \omega)], \quad (\text{A18})$$

$$\delta g_{d,C}(\omega) = l \hat{\mathbf{n}} \cdot [\delta\sigma_T(\omega) \vec{\Gamma}(\mathbf{r}, \omega) - \delta\sigma_C(\omega) \vec{\vec{C}}(\omega)] \cdot \hat{\mathbf{n}}. \quad (\text{A19})$$

The platform motion terms usually dominate over the ac gravity terms in these equations. The second term in Eq. (A19) constitutes an additional rotation induced error which must be added to the list considered in the previous section. The linear acceleration term in Eq. (A18) will be discussed in the following section along with other translation induced error sources.

Now, we briefly discuss $\delta\sigma_S(\omega)$ which arises from the failure to apply the wideband balance procedure. If the balance is attempted at a single frequency ω_b , Eq. (48) must be violated in general. Substituting Eqs. (46) into Eq. (A17a) and expanding it in a Taylor series, one finds

$$\delta\sigma_S(\omega) = \frac{2(\omega_b - \omega)\omega_b(\omega_{2c}^2 - \omega_{1c}^2)}{(\omega_{1c}^2 - \omega_b^2)(\omega_{2c}^2 - \omega_b^2)} + \delta\sigma_S(\omega_b), \quad (\text{A20})$$

where $\delta\sigma_S(\omega_b)$ is a residual balance error at ω_b . Although not essential, a highly symmetric gradiometer is convenient because $\omega_{2c} \simeq \omega_{1c}$ and, therefore, the wideband balance can be achieved with only two persistent currents I_1 and $I_2 \simeq I_1$ while keeping $i_1 = i_2 = 0$.

6. Linear motions of the platform

Although several sources of linear motion induced errors have been shown in the previous sections, it is instructive to combine these effects here. The linear velocity dependent Coriolis force term has been dropped in Eqs. (95) on the assumption that the proof masses are confined to move along the linear directions $\hat{\mathbf{n}}_1$ and $\hat{\mathbf{n}}_2$. A nonvanishing residual compliance in the directions perpendicular to the sensitive axes would allow the proof masses to respond to the transverse components of accelerations, thereby contributing to a velocity-dependent error. It is therefore important to design the suspension spring with high stiffness for all undesired degrees of freedom while obtaining a very weak spring in a linear direction. We will see in paper II how this condition is met in the actual design of the superconducting gradiometer.

It has been shown in Sec. 2 of this appendix that the modulation of Earth's gravity by a time-varying displacement error $\delta\rho(t)$ can be ignored because of the higher-order gradients involved. The dominant mechanisms which convert the linear vibrations of the platform into gradiometer errors are therefore (1) the sensitive axes misalignment $\delta\hat{\mathbf{n}}_-$, which couples the cross-component accelerations and (2) the scale factor mismatch $\delta\sigma_S(\omega)$, which couples the in-line component acceleration to the gradiometer output. Combining proper terms in Eqs. (A6b) and (A18), one finds

$$\delta g_{d,a}(\omega) = -[\delta\hat{\mathbf{n}}_- + \delta\sigma_S(\omega)\hat{\mathbf{n}}] \cdot \mathbf{a}(\mathbf{r}, \omega). \quad (\text{A21})$$

The two terms in this equation are related by the condition of the common mode balance. The balance is obtained in the real instrument by requiring $\delta g_{d,a}(\omega_b) = 0$ for a given applied acceleration, say, in the z direction:

$$\mathbf{a}(\mathbf{r}, \omega_b) = a(\omega_b)\hat{\mathbf{z}}. \quad (\text{A22})$$

Substitution of Eq. (A22) into Eq. (A21) leads to

$$\delta\sigma_S(\omega_b) = -\frac{\delta\hat{\mathbf{n}}_- \cdot \hat{\mathbf{z}}}{\hat{\mathbf{n}} \cdot \hat{\mathbf{z}}} + \delta\sigma_{S0}, \quad (\text{A23})$$

which can be substituted, in turn, into Eq. (A20) to obtain $\delta\sigma_S(\omega)$. Notice that, even with a wideband balance, $\delta\sigma_S(\omega) = \delta\sigma_S(\omega_b) \neq 0$ due to the misalignment of the sensitive axes and the residual balance error $\delta\sigma_{S0}$. The impossibility of obtaining a balance with an applied acceleration normal to $(\hat{\mathbf{n}}_1 + \hat{\mathbf{n}}_2)/2$ is indicated by the divergence of Eq. (A23), which occurs when $\hat{\mathbf{n}} \cdot \hat{\mathbf{z}} = 0$.

7. Scale factor nonlinearity and dynamic range

A nonlinear behavior of accelerometer scale factors arises from departure of the acceleration response of the

mechanical suspension springs from the linear behavior predicted by Hooke's law, higher-order terms in the modulation of the pancake coil inductances, L_a and L_b , higher order terms in the magnetic force F_{EM} , and, finally, nonlinearity in the current-to-voltage transfer function of the SQUID electronics. In Eqs. (14) we assumed perfect linearity of L_a and L_b as functions of the coil spacing. This assumption is clearly not rigorous because of the grain structure of the pancake coils and edge effects. The higher-order terms in F_{EM} , which are apparent in Eqs. (23) and (25), have been ignored in our attempt to linearize the circuit equations. Therefore, even if the mechanical springs and the SQUID electronics are constructed with sufficient linearity, the response of each accelerometer will be somewhat nonlinear due to the inevitable high-order response of the electrical circuit.

In analogy to Eqs. (A17) we define the *nonlinearity error* coefficients $h_{cc}(\omega)$, $h_{dd}(\omega)$, and $h_{cd}(\omega)$ by dividing the nonlinearity transfer functions $H_{G_i}^{cc}(\omega)$, $H_{G_i}^{dd}(\omega)$, and $H_{G_i}^{cd}(\omega)$, introduced in Eq. (101), by $H_{g_i}^d(\omega)$. Then the *equivalent* differential acceleration error due to scale factor nonlinearity can be written as

$$\begin{aligned} \delta g_{d,N}(\omega) = & h_{cc}(\omega)G_{cc}(\omega) + h_{dd}(\omega)G_{dd}(\omega) \\ & + h_{cd}(\omega)G_{cd}(\omega). \end{aligned} \quad (\text{A24})$$

Now, in most practical situations, the gravity terms are small compared to the platform motion terms in Eqs. (100) so that

$$G_{cc}(t) = [\hat{\mathbf{n}} \cdot \mathbf{a}(\mathbf{r}, t)]^2, \quad (\text{A25a})$$

$$G_{dd}(t) = l^2 \{ [\hat{\mathbf{n}} \cdot \boldsymbol{\Omega}(t)]^2 - \Omega^2(t) \}^2, \quad (\text{A25b})$$

$$G_{cd}(t) = l [\hat{\mathbf{n}} \cdot \mathbf{a}(\mathbf{r}, t)] \{ [\hat{\mathbf{n}} \cdot \boldsymbol{\Omega}(t)]^2 - \Omega^2(t) \}. \quad (\text{A25c})$$

It is clear that the Fourier transformation of these nonlinear functions of dynamic variables will down convert the wideband platform noise to the vicinity of dc, where the gravity gradient signal is to be detected. Therefore, it is imperative that the vibration and jitter noise of the apparatus be low-pass filtered before they reach the gradiometer. Detailed analysis of the noise down-conversion process will be given in paper II.

It is difficult to determine the nonlinearity error coefficients analytically. They can however be measured from the departures of the transfer functions $H_{g_i}^c(\omega)$ and $H_{g_i}^d(\omega)$ from the linear behavior. In principle, the nonlinearity in the two component accelerometers could also be matched. This would not, however, reduce all three error coefficients in Eq. (A24) to zero. A more powerful and practical approach to the problem is the linearization of the system by means of an electromechanical feedback. A feedback force, which is equal and opposite to the detected external force, can be applied to each proof mass so that the total force, the "error signal" for the feedback loop, is reduced by the inverse of the feedback gain. The reduction of the driving accelerations limits the actual displacement of each proof mass to a small amplitude, thereby reducing $\delta g_{d,N}(\omega)$. The error coefficients $h(\omega)$'s have therefore been effectively reduced. The average and differential feedback forces are direct measures of $g_c(t)$ and $g_d(t)$. The gradiometer thus measures the specific force

instead of the resulting displacement. The negative feedback comes with another important advantage, an increase in the *dynamic range* of the device. This so-called “force rebalance” feedback has been successfully applied to conventional inertial navigation instruments²⁷ and gravity gradiometers,⁷ although it is yet to be applied to superconducting gravity gradiometers.

One of the parameters responsible for the high sensitivity of the superconducting gradiometer is the low damping coefficient of the electromechanical springs. The low dissipation is necessarily accompanied with high- Q resonances of the modes which tend to amplify the acceleration noise at the resonance frequencies. An elegant way to take care of this problem is an active damping method²⁸ by which the Q 's are effectively lowered without increasing the Brownian motion noise level. The gradiometer response is narrowband filtered around the resonances, phase shifted by 90° , and fed back to the proof masses to actively drive down the resonant motions. This “cold damping” has been successfully demonstrated in superconducting gravity gradiometers.^{13,14}

8. Nonmechanical noise of the environment

It has been pointed out in the Introduction that superconductivity can be used to make a nearly perfect electromagnetic shield. In a practical superconducting shield with impurities, the Meissner effect does not exclude the magnetic field completely, but instead “freezes” some trapped magnetic field, thus providing a “perfect” shield against time-varying fields. One can combine high permeability shields with superconducting shields to attenuate both dc and ac electromagnetic fields as well as radiation very effectively. Therefore, the electromagnetic susceptibility of the superconducting gradiometer can be made negligible.

The thermal fluctuations of the environment could also be shielded by immersing the apparatus in superfluid helium, the Bose condensate phase of ^4He below 2.17 K. The nearly infinite heat conductivity and the large heat capacity of the superfluid provides a stable, gradient-free, thermal environment. Even normal fluid helium can provide an excellent thermal environment provided its vapor pressure is regulated. When the attenuation of the temperature fluctuations of the environment is not sufficient, one will have error terms that couple the temperature noise to the gradiometer output, as shown in Eq. (101). The fluctuation in the gradiometer temperature can cause error signals through its interaction with (1) the mechanical part and (2) the superconducting circuit.

In analogy to Eqs. (40), the temperature modulations of the two accelerometers, $T_1(\omega)$ and $T_2(\omega)$, are expressed in terms of their *common* and *differential temperatures*, $T_c(\omega)$ and $T_d(\omega)$:

$$T_1(\omega) = T_c(\omega) - \frac{1}{2}T_d(\omega), \quad (\text{A26a})$$

$$T_2(\omega) = T_c(\omega) + \frac{1}{2}T_d(\omega). \quad (\text{A26b})$$

The mechanically coupled temperature-induced error could arise simply from the thermal expansion of the base line:

$$\frac{\delta l(\omega)}{l} = \alpha(T)T_c(\omega), \quad (\text{A27})$$

where $\alpha(T)$ is the thermal expansion coefficient of the gradiometer body at the ambient temperature T . However, $\alpha(T)$ is extremely small for solids at liquid-helium temperatures so that the dimensional change $\delta l(\omega)$ is negligible in any practical situation.¹⁴ For the same reason, alignment changes $\delta \hat{n}_\pm(\omega)$ resulting from temperature fluctuations are negligible, demonstrating the *mechanical stability* of the cryogenic gravity gradiometer.

There is a more subtle coupling mechanism of the temperature noise through the mechanical part of the system. It is through the temperature dependence of Young's modulus $E(T)$ of the mechanical spring.²⁹ Since the stiffness of the suspension spring changes as a function of temperature, a temperature fluctuation will cause a displacement modulation when the spring is under stress either by gravity or by an unbalanced magnetic pressure. This can be seen in Eq. (25) for an *accelerometer*. When $\hat{n} \cdot \mathbf{g}_E(\mathbf{r}) \neq 0$ so that $x_0 \neq 0$, the temperature-induced modulation of ω_M^2 produces a first-order effect in displacement. It is convenient to move this term to the right-hand side of Eq. (25) and define an additional *effective* driving acceleration:

$$\delta g^T(t) = -[\omega_M^2(T + \delta T) - \omega_M^2(T)]x_0. \quad (\text{A28})$$

The proportionality of the spring constant $m\omega_M^2$ to $E(T)$ can be used to rewrite Eq. (A28) as

$$\delta g^T(t) = -\omega_M^2(T)x_0 \frac{1}{E(T)} \frac{dE}{dT} \delta T(t). \quad (\text{A29})$$

Substitution of Eq. (27) into Eq. (A29) and Fourier transformation leads to

$$g^T(\omega) = \left[g_E \cos \theta_n + \frac{\Lambda}{m} \left[I + \frac{1}{2} \frac{L_a - L_b}{L_a + L_b} i \right] i \right] \frac{1}{E(T)} \frac{dE}{dT} T(\omega). \quad (\text{A30})$$

It is clear from this equation that this effect can be eliminated by choosing i such that the quantity in the square brackets vanishes, i.e., by compensating the gravitational force with a magnetic levitation force.

In the actual operation of the gradiometer reported in paper II, $i \simeq 0$ was chosen so that the magnetic pressure term in Eq. (A30) was negligible. The temperature effect on the *gradiometer* can be found then by adding

$$g_c^T(\omega) = g_E \cos \theta_n \frac{1}{E(T)} \frac{dE}{dT} T_c(\omega), \quad (\text{A31a})$$

$$g_d^T(\omega) = g_E \cos \theta_n \frac{1}{E(T)} \frac{dE}{dT} T_d(\omega), \quad (\text{A31b})$$

to $g_c(\omega)$ and $g_d(\omega)$ in Eq. (41). It is assumed here that the two suspension springs of the proof masses have an identical Young's modulus $E(T)$. The temperature-induced current output can be written as

$$i_d^T(\omega) = H_{T_i}^c(\omega) T_c(\omega) + H_{T_i}^d(\omega) T_d(\omega), \quad (\text{A32})$$

where

$$H_{Ti}^c(\omega) = H_{gi}^c(\omega) g_E \cos \theta_n \frac{1}{E(T)} \frac{dE}{dT}, \quad (\text{A33a})$$

$$H_{Ti}^d(\omega) = H_{gi}^d(\omega) g_E \cos \theta_n \frac{1}{E(T)} \frac{dE}{dT}. \quad (\text{A33b})$$

Notice that the common temperature fluctuation $T_c(\omega)$ is balanced out to the same degree as the common acceleration. For a properly balanced gradiometer, therefore, this effect is expected to be negligible as long as $i \simeq 0$.

The second effect of the temperature noise, which acts on the superconducting circuit directly, comes from the temperature dependence of the ‘‘penetration depth’’ $\lambda(T)$ of the magnetic field in the superconductor:

$$\lambda(T) = \frac{\lambda(0)}{[1 - (T/T_0)^4]^{1/2}}, \quad (\text{A34})$$

where T_0 is the critical temperature for the superconductor. For niobium, $\lambda(0) = 5.0 \times 10^{-8}$ m and $T_0 = 9.2$ K. The variation of $\lambda(T_k)$ of the proof mass and pancake coils due to a temperature fluctuation $\delta T_k(t)$ of the k th acceleration transducer,

$$\delta \lambda(T_k) = \lambda(T_k + \delta T_k) - \lambda(T_k) \simeq \frac{d\lambda}{dT} \delta T_k, \quad (\text{A35})$$

modulates the superconducting inductances of Eq. (14) according to

$$L_{ka}(t) = L_{ka} + \Lambda(1 + \zeta) \delta \lambda(T_k) + \Lambda x_k^T(t), \quad (\text{A36a})$$

$$L_{kb}(t) = L_{kb} + \Lambda(1 + \zeta) \delta \lambda(T_k) - \Lambda x_k^T(t). \quad (\text{A36b})$$

Here

$$0 < \zeta < 1 \quad (\text{A37})$$

is the modulation efficiency of the penetration depth of the pancake coils. An approximation is made here that the sensing inductances are reasonably well matched so that distinction of ζ for each of these coils is not neces-

sary. In Eqs. (A36), $x_k^T(t)$ is the dynamic displacement produced in self-consistent response to the current modulations resulting from the temperature-induced inductance modulations. Given the penetration depth modulations, the displacement response $x_k^T(t)$ and the current response $i_d^T(t)$ are solved from the dynamical equations of the gradiometer. The dynamical equations and their solutions are modifications of those given in Sec. III.

Modifying Eqs. (18) and (19), the series are parallel inductances of the sensing coils L_{ka} and L_{kb} now becomes

$$L_{ks}(t) = L_{ks} + 2\Lambda(1 + \zeta) \delta \lambda(T_k), \quad (\text{A38})$$

$$L_{kp}(t) = L_{kp} + \frac{L_{ka}^2 + L_{kb}^2}{L_{ks}} \Lambda(1 + \zeta) \delta \lambda(T_k) - \frac{L_{ka} - L_{kb}}{L_{ks}} \Lambda x_k^T(t). \quad (\text{A39})$$

Flux quantization through the loops $L_{ka} + L_{kb}$ gives

$$I_k(t) = I_k \left[1 - \frac{2\Lambda(1 + \zeta) \delta \lambda(T_k)}{L_{ks}} \right]. \quad (\text{A40})$$

Substituting Eqs. (A38)–(A40) into the flux quantization condition for the loops $L_{kb}(t) + L_0$, which is generalized from Eq. (32), and taking Fourier transformation, one finds a modified version of Eq. (42):

$$x_k^T(\omega) + \alpha_k^T (1 + \zeta) \delta \lambda(T_k(\omega)) = \frac{L_{kp} + 2L_0}{\Lambda I_k'} \frac{1}{2} i_d^T(\omega) + (-1)^k \frac{L_{kp}}{\Lambda I_k'} i_c^T(\omega), \quad (\text{A41})$$

where the coefficients α_k^T are defined by

$$\alpha_k^T \equiv \frac{L_{ka} - L_{kb}}{L_{ks}} + \frac{L_{kp}}{L_{ks}} \frac{i_k}{I_k'}. \quad (\text{A42})$$

The homogeneous part of Eq. (25) generalized for $k=1,2$ is then solved using Eqs. (A38)–(A40) again, resulting in

$$\left[-\omega^2 + \omega_{kM}^2 + \frac{\Lambda^2 i_k^2}{m_k L_{ks}} \right] x_k^T(\omega) + \frac{\Lambda I_k'}{m_k} \frac{1}{2} i_d^T(\omega) + (-1)^k \frac{\Lambda I_k'}{m_k} i_c^T(\omega) = \frac{\Lambda^2 (I_k' + I_k) i}{m_k L_{ks}} (1 + \zeta) \delta \lambda(T_k(\omega)), \quad (\text{A43})$$

which are identical to Eqs. (41) with the driving gravity signal replaced by the $\delta \lambda(T_k)$ term on the right-hand side.

The relationships between the currents and $\delta \lambda$'s are obtained by eliminating x_k^T from Eqs. (A41) and (A43). The resulting pair of equations are the same as Eq. (43) on the left-hand side and have equal coefficients of $i_c^T(\omega)$ due to the common mode balance condition of Eq. (48). Therefore, the i_c^T terms are readily eliminated, yielding

$$i_d^T(\omega) = H_{gi}^d(\omega) (1 + \zeta) [\alpha_2^T (\omega_{2\lambda}^2 - \omega^2) \delta \lambda(T_2(\omega)) - \alpha_1^T (\omega_{1\lambda}^2 - \omega^2) \delta \lambda(T_1(\omega))], \quad (\text{A44})$$

where

$$\omega_{k\lambda}^2 \equiv \omega_{kM}^2 + \frac{\Lambda^2 i_k^2}{m_k L_{ks}} + \frac{\Lambda^2 (I_k' + I_k) i_k}{m_k \alpha_k^T L_{ks}}. \quad (\text{A45})$$

The temperature-induced output current can now be expressed in the form of Eq. (A32) with the identification

$$H_{Ti}^c(\omega) = H_{gi}^d(\omega) h_{Tc}(\omega), \quad (\text{A46a})$$

$$H_{Ti}^d(\omega) = H_{gi}^d(\omega) h_{Td}(\omega), \quad (\text{A46b})$$

where the temperature-error coefficients are obtained from Eqs. (A26), (A35), and (A44) as

$$h_{Tc}(\omega) = [\alpha_2^T (\omega_{2\lambda}^2 - \omega^2) - \alpha_1^T (\omega_{1\lambda}^2 - \omega^2)] (1 + \zeta) \frac{d\lambda}{dT}, \quad (\text{A47a})$$

$$h_{Td}(\omega) = \frac{1}{2} [\alpha_2^T(\omega_{2\lambda}^2 - \omega^2) + \alpha_1^T(\omega_{1\lambda}^2 - \omega^2)](1 + \xi) \frac{d\lambda}{dT} . \quad (\text{A47b})$$

In terms of these error coefficients, the *equivalent differential acceleration error due to temperature sensitivity* is

$$\delta g_{d,T}(\omega) = h_{T_c}(\omega) T_c(\omega) + h_{T_d} T_d(\omega) . \quad (\text{A48})$$

It is apparent from Eqs. (A42) and (A47a) that the effect of $T_c(\omega)$ is partially balanced by the match between pancake coil inductances L_{ka} and L_{kb} and by the common acceleration balance condition (48). On the other hand, $T_d(\omega)$ is usually negligible because the good thermal conductivity of the gradiometer body keeps the entire instrument in thermal equilibrium.

It has been pointed out¹⁸ that an exact common temperature balance could be achieved by adjusting the fourth persistent current i_2 with respect to I_1 , I_2 , and i_1 that are used for the wideband common acceleration balance. The

adjustments are iterated such that both the common acceleration balance condition (48) and the common temperature balance condition

$$\alpha_2^T(\omega_{2\lambda}^2 - \omega^2) = \alpha_1^T(\omega_{1\lambda}^2 - \omega^2) \quad (\text{A49})$$

are simultaneously satisfied. In practice, it will be easier to couple a separate superconducting loop, which senses only temperature, to the SQUID and adjust the persistent current in this loop to obtain the temperature balance. The advantage of the latter scheme is that the temperature and acceleration balances can be performed independently.

A slowly varying temperature of the environment, if uncompensated, can be an important source of a dc drift of the gradiometer. Such a drift, however, does not produce a random walk of the output, but the error is bounded because the dc level of the output is locked to the temperature of the gradiometer which is self-regulated to a large extent by the liquid helium itself.

*Present address: AT&T Bell Laboratories, Whippany, New Jersey 07981.

¹For a historical review of torsion balance experiments, see C. W. F. Everitt, in *Proceedings of the First Marcel Grossmann Meeting on General Relativity*, edited by R. Ruffini (North-Holland, Amsterdam, 1978), p. 548.

²For a historical introduction of room-temperature gravimeters, see J. E. Faller, in *Proceedings of the 1983 International School and Symposium on Precision Measurement and Gravity Experiment*, edited by W. T. Ni (Chuan Wen Book Co., Hsin-chu, Taiwan, 1983), p. 466.

³J. M. Goodkind, *Tectonophysics* **52**, 99 (1979).

⁴J. Weber, *Phys. Rev.* **117**, 306 (1960).

⁵See a review by J. A. Tyson and R. P. Giffard, *Annu. Rev. Astron. Astrophys.* **16**, 521 (1978).

⁶R. L. Forward, in *Proceedings of AIAA Unmanned Spacecraft Meeting* (AIAA, Los Angeles, California, 1965), p. 346.

⁷E. H. Metzger and D. R. Allen, Bell Aerospace Co. Report No. 9500-92044, 1972 (unpublished).

⁸M. B. Trageser, in *Proceedings of the First International Symposium on Inertial Technology for Surveying and Geodesy* (Canadian Institute of Surveying, Ottawa, Canada, 1977).

⁹H. J. Paik, *J. Appl. Phys.* **47**, 1168 (1976).

¹⁰*Spaceborne Gravity Gradiometers*, edited by W. C. Wells (NASA Conference Publication No. 2305, 1984).

¹¹J. W. Parke, H. J. Paik, H. A. Chan, and M. V. Moody, in *Proceedings of the Tenth International Cryogenic Engineering Conference*, edited by H. Collan *et al.* (Butterworth, Guildford, 1984), p. 361.

¹²H. J. Paik, E. R. Mapoles, and K. Y. Wang, in *Proceedings of Conference on Future Trends in Superconductive Electronics*, edited by B. S. Deaver *et al.* (Charlottesville, Virginia, 1978), p. 166.

¹³K. Y. Wang, Ph.D. thesis, Stanford University, Stanford, Cal-

ifornia, 1979.

¹⁴E. R. Mapoles, Ph.D. thesis, Stanford University, Stanford, California, 1981.

¹⁵H. J. Paik, *J. Astronaut. Sci.* **29**, 1 (1981).

¹⁶H. J. Paik, *IEEE Trans. Geosci. Remote Sensing* **GE-23**, 524 (1985).

¹⁷H. A. Chan, M. V. Moody, and H. J. Paik, *Phys. Rev. Lett.* **49**, 1745 (1982).

¹⁸H. A. Chan, Ph.D. thesis, University of Maryland, College Park, Maryland, 1982.

¹⁹K. R. Symon, *Mechanics*, 2nd ed. (Addison-Wesley, Reading, MA, 1961), p. 278.

²⁰H. J. Paik, *Phys. Rev. D* **19**, 2320 (1979).

²¹The term "acceleration signal" hereafter refers to the specific force $\mathbf{g}'(\mathbf{r}, t)$ defined in Sec. II.

²²The term "spectral density" refers to a *one-sided* spectral density in papers I and II unless specified otherwise.

²³J. N. Hollenhorst and R. P. Giffard, *J. Appl. Phys.* **51**, 1719 (1980).

²⁴M. V. Moody, H. A. Chan, H. J. Paik, and C. Stephens, in *Proceedings of 17th International Conference on Low Temperature Physics*, edited by U. Eckern *et al.* (North-Holland, Amsterdam, 1984), Vol. 2, p. 407.

²⁵H. A. Chan, M. V. Moody, H. J. Paik, and J. W. Parke, in *Proceedings of 17th International Conference on Low Temperature Physics* (Ref. 24), p. 927.

²⁶H. J. Paik, *Bull. Geod.* **55**, 370 (1981).

²⁷C. Broxmeyer, *Inertial Navigation Systems* (McGraw-Hill, New York, 1964).

²⁸C. Kittel, *Elementary Statistical Physics* (Wiley, New York, 1958), pp. 141–156.

²⁹J. W. Parke, H. J. Paik, E. R. Mapoles, W. M. Fairbank, and D. DeBra (unpublished).